

SANDIA REPORT

SAND97-8001 • UC-406

Unlimited Release

Printed November 1997

Modeling the In-plane Tension Failure of Composite Plates

Khanh V. Trinh

Prepared by

Sandia National Laboratories

Albuquerque, New Mexico 87185 and Livermore, California 94550

Sandia is a multiprogram laboratory operated by Sandia Corporation, a Lockheed Martin Company, for the United States Department of Energy under Contract DE-AC04-94AL85000.

Approved for public release; distribution is unlimited.



Sandia National Laboratories

Issued by Sandia National Laboratories, operated for the United States Department of Energy by Sandia Corporation.

NOTICE: This report was prepared as an account of work sponsored by an agency of the United States Government. Neither the United States Government nor any agency thereof, nor any of their employees, nor any of their contractors, subcontractors, or their employees, makes any warranty, express or implied, or assumes any legal liability or responsibility for the accuracy, completeness, or usefulness of any information, apparatus, product, or process disclosed, or represents that its use would not infringe privately owned rights. Reference herein to any specific commercial product, process, or service by trade name, trademark, manufacturer, or otherwise, does not necessarily constitute or imply its endorsement, recommendation, or favoring by the United States Government, any agency thereof, or any of their contractors or subcontractors. The views and opinions expressed herein do not necessarily state or reflect those of the United States Government, any agency thereof, or any of their contractors.

Printed in the United States of America. This report has been reproduced directly from the best available copy.

Available to DOE and DOE contractors from
Office of Scientific and Technical Information
P.O. Box 62
Oak Ridge, TN 37831

Prices available from (615) 576-8401, FTS 626-8401

Available to the public from
National Technical Information Service
U.S. Department of Commerce
5285 Port Royal Rd
Springfield, VA 22161

NTIS price codes
Printed copy: A04
Microfiche copy: A01

Modeling the In-plane Tension Failure of Composite Plates

Khanh V. Trinh
Structural & Thermomechanical Modeling Department
Sandia National Laboratories/California

ABSTRACT

This study developed a modeling method to predict the final failure load of laminated composite plates which may contain cutouts and are subjected to quasi-static in-plane tensile loads. The modeling method uses an existing finite element code together with a progressive damage model (progressive damage analyses) that was developed from existing composite failure models. This study focused on overcoming numerical problems often encountered in analyses that exhibit significant stable damage growth in the composite materials. These numerical problems limit progressive damage analyses to problems with simple loading and geometry. These numerical problems must be overcome to make this modeling approach practical.

To keep the computational cost at a reasonable level, the modeling method uses a quasi-static solution procedure to solve composite plate problems with quasi-static load. The numerical problems in the quasi-static analyses are nonconvergence problems caused by the discontinuous material behavior from brittle fiber failure. This study adds artificial damping to the material model to suppress the discontinuous material behavior. The artificial damping essentially changes the material behavior, and could adversely change the final failure load prediction. Thus, a selective scheme for adding the damping was developed to minimize adverse damping effects. In addition, this modeling method uses multiple analyses at different levels of artificial damping to determine damping effects on the failure load prediction.

Fracture strength experimental data for small coupons with small cutouts and large panels with larger cutouts available in the literature were selected and used to verify failure predictions of the developed modeling method. Results show that, without the artificial damping treatment, progressive damage analyses reasonably predicted the fracture strength of the small coupons, but severely underpredicted the fracture strength of the large panels. With the artificial damping treatment, the analyses predicted the failure load of both the small coupons and the large panels reasonably well.

Acknowledgments

I would like to thank Professor Fu-Kuo Chang of Stanford University for his guidance and encouragement over the years. His guidance and advice were invaluable and much appreciated. I would also like to thank Professor George S. Springer and Professor Richard M. Christensen for their advice and review of this work.

I would like to thank my peers in the Structures and Composites Laboratory, Stanford University, for their assistance and friendship. And finally, I would like to express my appreciation for the support of Sandia National Laboratories.

Contents

| | Page |
|--|------------|
| CHAPTER 1 INTRODUCTION | 1-1 |
| 1.1 Motivation and Objective | 1-1 |
| 1.2 Current Technology and Research Focus | 1-1 |
| CHAPTER 2 PROBLEM STATEMENT | 2-1 |
| CHAPTER 3 METHOD OF APPROACH | 3-1 |
| CHAPTER 4 COMPOSITE FAILURE MODELING | 4-1 |
| 4.1 Modeling Overview | 4-1 |
| <i>Failure Modes</i> | 4-2 |
| 4.2 Constitutive Modeling | 4-3 |
| <i>Matrix Cracking</i> | 4-3 |
| <i>Fiber Breakage</i> | 4-5 |
| <i>Fiber-Matrix Shearing</i> | 4-6 |
| 4.3 Failure Prediction | 4-7 |
| <i>Fiber Breakage</i> | 4-7 |
| <i>Matrix Cracking</i> | 4-7 |
| <i>Fiber-Matrix Shearing Failure</i> | 4-7 |
| CHAPTER 5 NONCONVERGENCE PROBLEMS | 5-1 |
| 5.1 Numerical Problems in Composite Progressive Failure Analysis | 5-1 |
| 5.2 Material Characteristics and Nonconvergence Problems | 5-5 |
| CHAPTER 6 ARTIFICIAL DAMPING MODEL | 6-1 |
| 6.1 Artificial Damping Model | 6-1 |
| 6.2 Modeling Strategy | 6-6 |
| 6.3 Material Model Implementation | 6-8 |
| CHAPTER 7 MODEL VERIFICATION | 7-1 |
| 7.1 Small Coupon Verification | 7-1 |
| <i>Experimental Data</i> | 7-1 |
| <i>Progressive Damage Analysis</i> | 7-3 |
| <i>Failure Load Comparison</i> | 7-7 |
| <i>Artificial Damping Effects on Failure Load Prediction</i> | 7-8 |
| 7.2 Large Panel Verification | 7-9 |
| <i>Experimental Data</i> | 7-10 |
| <i>Progressive Damage Analyses</i> | 7-11 |
| <i>Failure Load Comparison</i> | 7-14 |
| <i>Artificial Damping Effects on Failure Load Prediction</i> | 7-15 |
| CHAPTER 8 SUMMARY AND DISCUSSIONS | 8-1 |
| APPENDIX A—EXTENSIONAL VISCOUS STIFFNESS MATRIX | A-1 |
| APPENDIX B—USING PDLAM WITH ABAQUS/STANDARD | B-1 |
| B.1 Overview | B-1 |
| B.2 Preprocessing for PDLAM | B-1 |
| B.3 ABAQUS Input File Preparation for PDLAM | B-2 |
| REFERENCES | R-1 |

Illustrations

| No. | | Page |
|------|--|------|
| 2-1 | Schematic of the modeling problem..... | 2-1 |
| 4-1 | On-axis (x, y, z) and off-axis (x_1, x_2, x_3) coordinate systems | 4-2 |
| 4-2 | ϕ measures spacing of matrix crack..... | 4-4 |
| 5-1 | Example 5A: quasi-isotropic plate under uniaxial tension | 5-4 |
| 5-2 | Displacement jump due to fiber failure in 45 plies | 5-5 |
| 5-3 | Stiffness degradations due to matrix cracking 90° plies..... | 5-7 |
| 5-4 | Example 5B: [± 45]s under uniaxial Tension | 5-8 |
| 5-5 | Stiffness degradations due to fiber-matrix shear failure are relatively gradual..... | 5-8 |
| 6-1 | 1D spring and dashpot representation of the 1D model | 6-3 |
| 6-2 | Stress surface of the 1D model | 6-3 |
| 6-3 | Artificial damping distribution..... | 6-6 |
| 6-4 | Typical damping effects on failure load prediction | 6-7 |
| 6-5 | Secant method to model brittle failure..... | 6-11 |
| 6-6 | Flow chart of material model subroutine | 6-14 |
| 7-1 | Small coupon test configuration | 7-2 |
| 7-2 | Small coupon test geometries..... | 7-2 |
| 7-3 | Boundary condition and displacement controlled load condition | 7-4 |
| 7-4 | Finite element meshes for small coupon analyses (not to scale)..... | 7-6 |
| 7-5 | Fracture strength comparison for small coupons..... | 7-8 |
| 7-6 | Damping effects on small coupon failure prediction | 7-9 |
| 7-7 | Schematic of large panel under uniaxial tension load..... | 7-10 |
| 7-8 | Large panel under biaxial tension tests | 7-11 |
| 7-9 | Biaxial mesh | 7-12 |
| 7-10 | Fracture strength comparison for large panels..... | 7-15 |
| 7-11 | Damping effects on large panel failure predictions..... | 7-16 |
| A-1 | On-axis (x, y, z) and off-axis (x_1, x_2, x_3) coordinate systems | A-1 |
| A-2 | Laminate's z coordinate (thickness direction) | A-6 |

Tables

| No. | | Page |
|------------|--|-------------|
| 7-1 | Small Coupon Test Cases..... | 7-3 |
| 7-2 | Properties and Parameters Used in Small Coupon Analyses..... | 7-5 |
| 7-3 | Failure Load Comparison for Small Coupons | 7-7 |
| 7-4 | Large Panels Under Uniaxial Tension Test Cases | 7-10 |
| 7-5 | Biaxial Panel Test Cases | 7-11 |
| 7-6 | Properties and Parameters Used in Large Panel Analyses | 7-13 |
| 7-7 | Failure Load Comparison for Large Panels | 7-14 |
| B-1 | External Files Required for PDLAM | B-1 |
| B-2 | Data for PDLAM Through ABAQUS Input File..... | B-3 |

List of Symbols

| | |
|-------------------|---|
| a | crack half length |
| E_{xx} | ply longitudinal modulus |
| E_{yy} | ply transverse modulus |
| G_{xy} | ply in-plane shear modulus |
| G_{xz} | ply out-of-plane shear modulus |
| G_{yz} | ply out-of-plane shear modulus |
| G_{Ic}, G_{IIc} | critical intralaminar mode I and mode II fracture toughness, respectively |
| l | half length of the matrix crack spacing |
| $\{q\}$ | vector of nodal displacements |
| $[Q]$ | in-plane on-axis stiffness matrix for a unidirectional ply |
| $[Q(\Phi)]$ | in-plane on-axis stiffness matrix of a ply as a function of crack density Φ in the ply |
| S | effective shear strength of an undamaged ply |
| $S(\Phi)$ | effective shear strength of a ply as a function of crack density Φ in the ply |
| t | thickness of laminate |
| t_n | thickness of the n th ply group |
| $[T]$ | transformation matrix of stress and strain vectors |
| W | width of laminate |
| X_t | longitudinal tensile strength of a unidirectional composite |
| Y_t | effective transverse tensile strength of an undamaged ply |
| $Y_t(\Phi)$ | effective transverse tensile strength of a ply as a function of crack density Φ in the ply |

Greek Letters

| | |
|---------------|--|
| α | material shear nonlinearity parameter |
| δ | critical fiber interaction length |
| γ_{xy} | engineering shear strain |
| λ | parameter in the bolt bearing damage model |
| Φ | matrix crack density |
| Φ_0 | saturation matrix crack density |
| ν_{xy} | Poisson's ratio |
| τ_{xy} | in-plane ply shear stress |

| | |
|---------------|--|
| θ | ply orientation angle (direction of the fibers with respect to the off-axis coordinate system) |
| ξ, η | natural coordinates for each finite element |
| σ_r | x_r — <i>direction ply stress</i> |
| σ_z | x_z — <i>direction ply stress</i> |
| σ_x | x_r — <i>direction ply stress</i> |
| σ_y | x_r — <i>direction ply stress</i> |
| σ_6 | x_r — <i>direction ply stress</i> |
| σ_{xx} | fiber direction ply stress |
| σ_{yy} | transverse ply stress |
| -1 | denotes inverse |
| $1, 2, 3$ | denotes laminate global coordinate directions |
| b | denotes bearing damage in degraded ply stiffness matrix |
| c | denotes compression |
| t | denotes tension |
| x, y, z | denotes on-axis ply coordinate directions |
| f^+ | denotes fiber breakage in degraded ply stiffness matrix |
| f^- | denotes fiber-matrix compression in degraded ply stiffness matrix |
| m^+ | denotes matrix cracking in degraded ply stiffness matrix |
| m^- | denotes matrix compression in degraded ply stiffness matrix |
| n | denotes matrix compression in degraded ply stiffness matrix |
| O, o | denotes initial (reference) configuration |
| s | denotes fiber-matrix shearing in degraded ply stiffness matrix |
| (t) | denotes Newton-Raphson iteration number |
| T | denotes transpose |

Miscellaneous

| | |
|---------------|--|
| Σ | summation operator |
| $d^n \Gamma$ | differential surface area at configuration n |
| $d^n v$ | differential volume at configuration |
| $\ \cdot \ $ | denotes Euclidean norm |

This page intentionally left blank

Chapter 1

Introduction

1.1 Motivation and Objective

Effective modeling methods for predicting the fracture strength of laminated composite plates containing cut-outs and subjected to in-plane tensile loads are important composite modeling tools. These modeling tools can be used to estimate the damage tolerance of composite structures including aircraft fuselages, rocket motor cases, various types of tanks, containers and pipes. The damage tolerance of a structure is used to establish damage and flaw limits allowed in the structure for a specific period of unrepaired usage [1,2]. For composite structures, the damage tolerance is usually a major design and cost driver, especially in high performance aerospace applications where safety and reliability are critical [3-6].

1.2 Current Technology and Research Focus

Because of the significance of the problem, extensive work has been done on this subject. Numerous analytical models have been proposed to predict the tensile fracture strength of composite laminates with cut-outs [7]. These models can be divided into two groups: semiempirical criteria and comprehensive numerical methods. The semiempirical criteria are experimentally expensive. The comprehensive numerical methods are computationally intensive.

The semiempirical criteria are simple equations that will predict the tensile fracture strength of notched laminates for a given loading and geometry [8-14]. These criteria are easy to use, but require the determination of one or more “characteristic parameters” from laboratory experiments. These empirical parameters account for the combined effects of the material, the lay-up, the loading, and the geometry of the problem. Examples of more popular semiempirical fracture models include the linear elastic fracture mechanics based criterion by Waddoups-Eisenmann-Kaminski [8], the Point Stress and Average Stress criterion by Whitney and Nuismer [9,10], the strain based criterion by Poe-Sova [11,12], and the Mar-Lin criterion [13].

Most of the semiempirical fracture criteria work has concentrated on coupons with relatively small notches, having sizes less than 2 inches [4,7,15]. These semiempirical criteria can predict the fracture strength of small notches reasonably well. However, the accuracy of the fracture predictions decreases significantly when these methods are extrapolated to predict the fracture strength of larger notch sizes [3,4,5]. The Mar-Lin criteria improves the accuracy of the fracture strength in larger notch sizes by using an additional parameter related to the order of the notch tip singularity. This

additional parameter may require expensive experiments involving larger notch sizes [16,17]

One disadvantage of these semiempirical criteria is that they are only applicable to problems with very simple loading and geometry since the effects of the loading and the geometry are accounted for by the “characteristic parameters.” Most existing semiempirical criteria work has concentrated on flat, rectangular plates containing a circular notch or a horizontal slit and subjected to a uniaxial tension load [7,15]. These semiempirical criteria may not be suitable for more complex structures such as stiffened plates or more general in-plane loads, including the biaxial membrane load of a pressure vessel.

Comprehensive numerical methods use finite element analyses together with a composite damage material model (progressive failure analyses) to predict the fracture strength of notched composite laminates [16–20]. These methods are computationally intensive. The finite element analyses are much more difficult, more time consuming, and more expensive to perform than the semiempirical fracture criteria. On the other hand, most of these numerical methods do not require expensive laboratory experiments to determine “characteristic parameters.” Most damage models used in these numerical methods may require experiments to determine material properties and model parameters. However, these experiments are typically performed at the ply level, and thus are much easier and cheaper to do. These numerical methods are also more suitable for more complex geometry and loading problems since the geometry and the loading are accounted for by the mesh and the boundary condition of the finite element analyses.

Similar to the semiempirical criteria work, most existing progressive failure analysis work has also concentrated on small coupons containing relatively small notch sizes and subjected to a uniaxial tension load. Existing progressive failure modeling methods can reasonably predict the fracture strength for these problems [21,22]. However, when applied to larger notch size and/or more complex loading and geometry, the finite element analyses will often prematurely terminate due to numerical problems. These problems prevent the analyses from obtaining reasonable fracture strength predictions.

Progressive failure analyses involve degrading material properties when failures are detected. The composite materials considered in this research are brittle material systems, such as graphite/epoxy, kevlar/epoxy and fiberglass/epoxy. Failure responses in these materials exhibit highly nonlinear and discontinuous behaviors. These material behaviors often cause severe numerical difficulties in the finite element analyses.

In coupons containing small notch sizes under uniaxial loading, there is usually very little damage accumulation before the final failure occurs. The little damage accumulation causes less numerical difficulties in the ensuing finite element analyses. Thus, some of these analyses can achieve the final failure prediction. Furthermore, since small damage accumulations mean relatively little failure progressions, even if numerical problems terminated these analyses before the final failure, notch strength predictions based on the maximum analysis load can often be made without great loss of accuracy.

For plates with larger notch sizes, experiments have shown that the cumulative damage can grow to a substantially larger area with increased applied load before final failure occurs [5,16]. The extensive damage could significantly reduce material properties in a larger area and potentially causes more numerical problems. Furthermore, larger damaged areas mean more failure progression. This means the highest analysis load cannot be confidently used to predict the plate's fracture strength in analyses that terminated prematurely due to numerical problems. For larger notch sizes, numerical problems must be overcome to obtain reasonable notch strength predictions. Since the geometry of more realistic modeling problems will generally be more complex than those considered in existing progressive damage modeling work, existing comprehensive modeling methods for predicting the fracture strength of composite plates are not effective for practical applications.

This page intentionally left blank

Chapter 2 Problem Statement

Consider laminated composite plates with or without a cutout and subjected to an in-plane load as depicted in Figure 2-1. The geometry of the plates and the cutouts can be arbitrary. The ply orientation of the laminate can be arbitrary, but must be symmetric with respect to its mid-plane. For a given lay-up, material system, and loading condition, it is desirable to determine the final failure load.

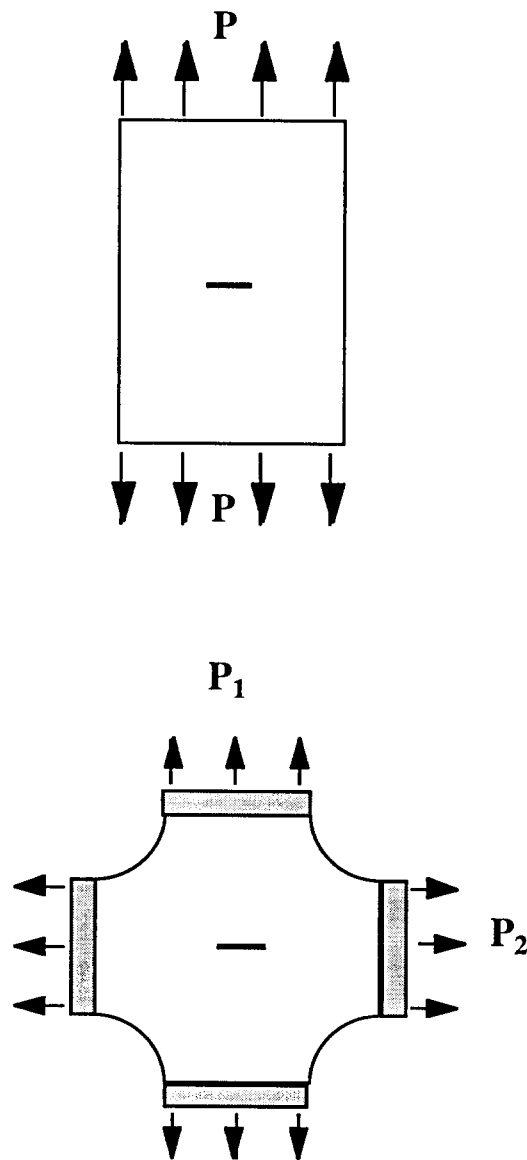


Figure 2-1. Schematic of the modeling problem.

This page intentionally left blank

Chapter 3

Method of Approach

The objective of this research was to develop an effective analytical method for predicting the fracture strength of composite plates containing cutouts and subjected to in-plane tensile loads. This study adopted the approach that uses finite element analyses together with a progressive damage model. In order to achieve the objective, the modeling method must have three working components: the finite element modeling, the composite failure modeling, and treatments for the numerical problems in the finite element analyses.

Since existing comprehensive modeling methods can reasonably predict the fracture strength of coupons with small notch sizes subjected to simple loading, it was assumed that existing finite element modeling methods and existing composite progressive damage models are adequate for the objective of this study. Thus, to simplify this research and to make use of existing finite element technologies, the commercial general purpose finite element code ABAQUS/Standard [23] was used to perform the finite element analyses. In addition, a progressive damage model was developed based on existing work to model composite materials. This approach allowed the current study to focus on overcoming numerical problems that prevent the analyses from making reasonable fracture strength predictions.

The modeling method developed in this study uses quasi-static finite element analyses to predict the fracture strength of notched composite plates. The finite element meshes account for the geometry of the plates. In the analyses, the load is applied incrementally, and the material properties are degraded progressively as failures occur. Final failure is predicted when the damaged plates can no longer sustain the applied loads.

The developed composite damage model assumes that the material behaviors can be characterized as functions of the material damaged state. Damage initiation and growth are predicted based on the stress state of the material and various failure criteria. The model assumes that damaged composites can be treated as a continuous elastic body with degraded material properties. Chapter 4 describes the constitutive modeling and the damage growth criteria used in the material model.

Composite failures include brittle failures. These brittle failures are the root causes of the numerical problems. Chapter 5 discusses these numerical problems and also describes material behaviors defined by the damage model that may lead to these numerical problems.

This study adds artificial damping to the material model to overcome numerical problems. The artificial damping smoothes out the discontinuous failure behaviors of the composites. The damping essentially changes the plate response in the analyses and may have an effect on the fracture strength prediction. This artificial damping technique only works when the damping effect on the fracture strength prediction is insignificant. The developed modeling method uses parametric studies to determine effects of the artificial damping on the fracture strength prediction. Chapter 6 describes the artificial damping model, along with the modeling method and strategy required for this artificial damping model.

Experimental fracture strength data was selected from the literature to verify the developed modeling method. These fracture test data included coupons with small notches and panels with larger notches. These fracture test data also included both uniaxial tension load and biaxial tension load. Chapter 7 compares failure load predictions between test data and model predictions. Chapter 8 gives a summary of this study, and discusses the applicability of the developed modeling method.

Chapter 4

Composite Failure Modeling

To predict the in-plane tensile fracture of composite laminates, the modeling method developed in the current study requires a finite element code, a suitable composite damage model, and treatments for nonconvergence problems caused by brittle composite failures. The commercial finite element code ABAQUS/Standard [23] was used to perform the analyses. This study also developed a material model based on a damage model recently proposed by Shahid and Chang to predict failures in laminated composites subjected to in-plane tensile and shear loads [21]. This chapter describes the developed damage model.

4.1 Modeling Overview

This study only considered unidirectional composite laminates. Layered shells are used to model the composite laminates. A layer can represent a ply or a ply group.

The developed modeling method uses layered plates [24-26] to model the composite laminates. A layer can represent a ply or a ply group. The layers are modeled simply as a homogeneous material with orthotropic properties [27]. The layers can have different thicknesses, different principle directions, and different material behavior. The basic material constitutive relations are defined at the layer level. The total laminate stiffness is calculated using classical lamination theory [24].

At the layer level, the material model treats undamaged layers as elastic materials. The material model treats layers containing damages also as continuous elastic materials with degraded properties. Thus, elastic relations hold for both undamaged and damaged material. Figure 4-1 shows coordinate systems used to describe unidirectional composites.

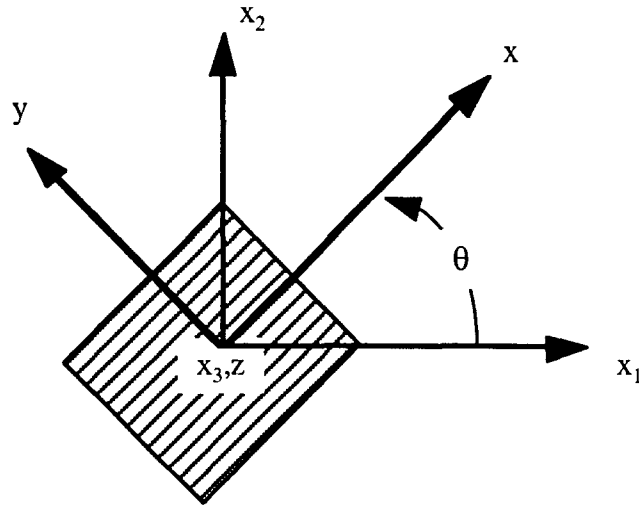


Figure 4-1. On-axis (x, y, z) and off-axis (x_1, x_2, x_3) coordinate systems.

In a layer, the basic on-axis constitutive relations are as follows:

$$\begin{pmatrix} \bar{\sigma}_{xx} \\ \bar{\sigma}_{yy} \end{pmatrix} = \begin{pmatrix} Q_{xx}^D & Q_{xy}^D \\ Q_{yx}^D & Q_{yy}^D \end{pmatrix} \begin{pmatrix} \bar{\epsilon}_{xx} \\ \bar{\epsilon}_{yy} \end{pmatrix} \quad (4.1)$$

$$\bar{\gamma}_{xy} = \frac{\bar{\sigma}_{xy}}{G_{xy}^D} + \alpha \left(\frac{\bar{\sigma}_{xy}}{G_{xy}^D} \right)^3 \quad (4.2)$$

where $\bar{\sigma}_{ij}, \bar{\epsilon}_{ij} (i, j = x, y)$ and $\bar{\gamma}_{xy}$ are the ply effective stresses and strains in the ply coordinate system. Q_{ij}^D and G_{xy}^D are the effective stiffnesses of the degraded ply. α is the parameter originally proposed by Tsai and Hahn to model the highly nonlinear shear stress to shear strain relationship in unidirectional composites [28]. Tsai and Hahn developed Equation 4.2 for unidirectional composites without damage.

Failure Modes

Failures in composite materials are complex and involve many modes. In predicting the fracture strength of notched plates subjected to in-plane tensile and shear

1. *fiber breakage* dominated failure mode
2. *matrix cracking* dominated failure mode
3. *fiber-matrix shearing* dominated failure mode

The damage material model consists of two main parts: constitutive modeling and failure prediction. The constitutive modeling defines stress-strain relations in the plies as functions of the material damage state. The failure prediction predicts damage initiation and growth in the material.

4.2 Constitutive Modeling

For the constitutive modeling, the material model treats both undamaged and damaged layers as homogeneous and elastic materials. Equations 4.1 and 4.2 define the stress-strain relations as functions of effective stiffnesses Q_{ij}^D , G_{xy}^D and the shear nonlinearity constant α . The effective stiffnesses are functions of the material damage state. The damage state is defined by the extent of failure in each of the three failure modes considered. Each failure mode degrades the material differently. These degradations are cumulative. Therefore, the effective stiffness components are calculated by combining the degradation from each of the three failure modes. The following subsections describe the material degradation from each of the three failure modes considered.

Matrix Cracking

Matrix cracks may form in laminated composites subjected to in-plane tensile or shear load [46,47]. These cracks will degrade the materials. Based on the theory of elasticity and fracture mechanics, Shahid and Chang proposed a model that will calculate the effective stiffnesses $Q_{ij}(\phi)$ and $G_{xy}(\phi)$, the matrix tensile strength $Y_t(\phi)$, and the in-plane shear strength $S(\phi)$ of each lamina in a symmetric laminate as functions of the crack density. Expressions for $Q_{ij}(\phi)$, $G_{xy}(\phi)$, $Y_t(\phi)$, and $S(\phi)$ can be found in Reference [21]. In Shahid's model, the crack density, ϕ , measures the crack spacing perpendicular to the fiber direction, and is defined as:

$$\phi = \frac{1}{2l} \quad (4.3)$$

where $2l$ is the distance between two adjacent cracks as shown in Figure 4-2. ϕ indicates the extent of matrix cracking damage in the material.

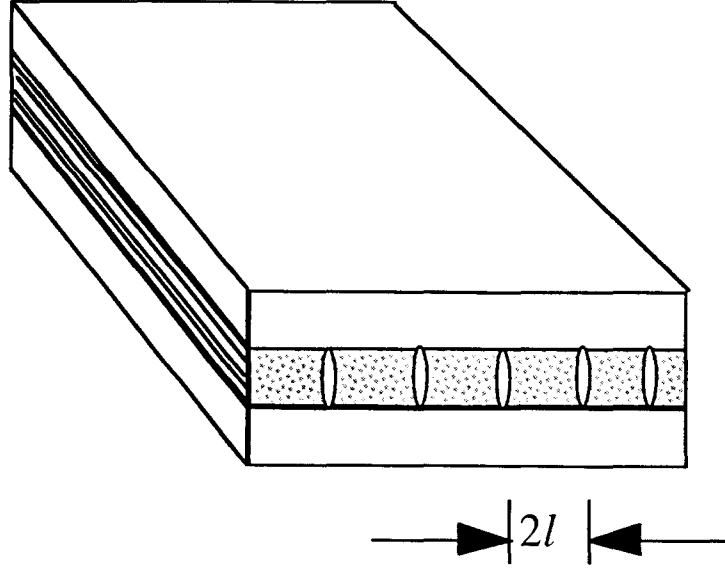


Figure 4-2. ϕ measures spacing of matrix crack.

When the matrix cracking failure criteria is satisfied at a material point, the degraded stress-strain relations are as follows:

$$\begin{pmatrix} \bar{\sigma}_{xx} \\ \bar{\sigma}_{yy} \end{pmatrix} = \begin{pmatrix} Q_{xx}^m(\phi) & Q_{xy}^m(\phi) \\ Q_{yx}^m(\phi) & Q_{yy}^m(\phi) \end{pmatrix} \begin{pmatrix} \bar{\epsilon}_{xx} \\ \bar{\epsilon}_{yy} \end{pmatrix} \quad (4.4)$$

$$\bar{\gamma}_{xy} = \frac{\bar{\sigma}_{xy}}{G_{xy}^m(\phi)} + \alpha \left(\frac{\bar{\sigma}_{xy}}{G_{xy}^m(\phi)} \right)^3 \quad (4.5)$$

where $Q_{xx}^m(\phi)$ and $G_{xy}^m(\phi)$ are the effective degraded stiffnesses due to the matrix cracking failure mode. These stiffnesses are defined as:

$$[Q(\phi)]^m = \begin{pmatrix} Q_{xx}(\phi) & Q_{xy}(\phi)d_s \\ Q_{yx}(\phi)d_s & Q_{yy}(\phi)d_s \end{pmatrix} \quad (4.6)$$

$$G_{xy}^m = G_{xy}(\phi) \quad (4.7)$$

where d_s is the matrix cracking failure degradation factor, and is defined as follows:

$$d_s = 1 \quad \text{when} \quad \bar{\epsilon}_{yy} < \bar{\epsilon}_{yy}^0 \quad (4.8)$$

$$d_s = 1 \quad \text{when} \quad \bar{\epsilon}_{yy} \geq \bar{\epsilon}_{yy}^0 \quad (4.9)$$

where $\bar{\epsilon}_{yy}^0$ is the matrix tensile failure strain of a unidirectional ply. When $\bar{\epsilon}_{yy} \geq \bar{\epsilon}_{yy}^0$, Q_{xy}^m , Q_{yx}^m and Q_{yy}^m are degraded to 0.

Fiber Breakage

The degraded on-axis stress-strain relations for the fiber breakage failure mode are as follows:

$$\begin{pmatrix} \bar{\sigma}_{xx} \\ \bar{\sigma}_{yx} \end{pmatrix} = \begin{pmatrix} Q_{xx}^f(\phi) & Q_{xy}^f(\phi) \\ Q_{yx}^f(\phi) & Q_{yy}^m(\phi) \end{pmatrix} \begin{pmatrix} \bar{\epsilon}_{xx} \\ \bar{\epsilon}_{yy} \end{pmatrix} \quad (4.10)$$

$$\bar{\gamma}_{xy} = \frac{\bar{\sigma}_{xy}}{G_{xy}^f(\phi)} + \alpha \left(\frac{\bar{\sigma}_{xy}}{G_{xy}^f(\phi)} \right)^3 \quad (4.11)$$

where $Q_{ij}^f(\phi)$ for $i, j = x, y$ and $G_{xy}^f(\phi)$ are the effective degraded stiffnesses due to the fiber breakage failure mode. These stiffnesses are defined as:

$$[Q(\phi)]^f = \begin{pmatrix} Q_{xx}(\phi)d_f & Q_{xy}(\phi)d_f \\ Q_{yx}(\phi)d_f & Q_{yy}(\phi)d_f \end{pmatrix} \quad (4.12)$$

$$G_{xy}^f = G_{xy}(\phi)d_f \quad (4.13)$$

where d_f is the fiber failure degradation factor, and is defined as follows:

$$d_f = 1 \quad \text{when} \quad A_f > \delta^2 \quad (4.14)$$

$$d_f = 0 \quad \text{when} \quad A_f \leq \delta^2 \quad (4.15)$$

where A_f is the extent of the fiber failure area over which the stress is equal to or higher than the longitudinal tensile strength, X_{fT} , of the composites. δ is the fiber

interaction length of the unidirectional composite considered. When $A_f \geq \delta^2$, the failed ply loses all of its stiffness abruptly.

By assuming a rigid-perfect plastic behavior of the matrix at the fiber-matrix interface and applying the fiber bundle theory [29-31], Tsai and Hahn proposed to estimate δ as follows [24]:

$$\delta = 2d \left(\frac{X_f}{4\tau_y} \right)^{\frac{\omega}{\omega+1}} \left[\frac{(\omega+1)L}{d} \right]^{\frac{1}{\omega+1}} \quad (4.16)$$

where d is the diameter of the fibers, X_f is the average fiber strength, and τ_y is the yielding stress of the matrix. L is the length of the fibers under consideration (typically one inch long). ω is the shape parameter of the Weibull distribution of the fiber strength distribution.

δ calculated from Equation 4-16 can only be used as an approximation due to assumptions made and variations of the material parameters required. Values for δ range from 0.025 to 0.06 for typical graphite/epoxy composites[22].

Fiber-Matrix Shearing

When the in-plane shear failure criteria is satisfied at a material point, stiffness components will be degraded as follows:

$$\begin{pmatrix} \bar{\sigma}_{xx} \\ \bar{\sigma}_{yy} \end{pmatrix} = \begin{pmatrix} Q_{xx}^s(\phi) & Q_{xy}^s(\phi) \\ Q_{yx}^s(\phi) & Q_{yy}^s(\phi) \end{pmatrix} \begin{pmatrix} \bar{\epsilon}_{xx} \\ \bar{\epsilon}_{yy} \end{pmatrix} \quad (4.17)$$

$$\bar{\gamma}_{xy} = \frac{\bar{\sigma}_{xy}}{G_{xy}^s(\phi)} + \alpha \left(\frac{\bar{\sigma}_{xy}}{G_{xy}^s(\phi)} \right)^3 \quad (4.18)$$

where $Q_{xx}^s(\phi)$ and $G_{xy}^s(\phi)$ are the effective degraded stiffnesses due to the fiber-matrix shearing failure mode. These stiffnesses are defined as:

$$[Q(\phi)]^s = \begin{pmatrix} Q_{xx}(\phi) & Q_{xy}(\phi) \\ Q_{yx}(\phi) & Q_{yy}(\phi) \end{pmatrix} \quad (4.19)$$

$$G_{xy}^s = G_{xy}(\phi)d_s \quad (4.20)$$

where d_s is the degradation factor defined by Equations 4.8 and 4.9.

4.3 Failure Prediction

Fiber Breakage

The failure criteria for this failure mode is the maximum stress criteria: [32]

$$\frac{\bar{\sigma}_{xx}}{X_t} \geq 1 \quad (4.21)$$

where $\bar{\sigma}_{xx}$ is the effective longitudinal stress of the ply under consideration, and X_t is the longitudinal tensile strength of the unidirectional composites. The fiber breakage dominated failure mode is the most severe of the three failure modes considered. When Equations. 4-21 and 4.15 are satisfied, the material loses all of its load-carrying capability from then on.

Matrix Cracking

The failure criteria for the matrix cracking failure mode is a modified Hashin's criterion [33], and is as follows:

$$\left(\frac{\bar{\sigma}_{yy}}{Y_t(\phi)} \right)^2 + \left(\frac{\bar{\sigma}_{xy}}{S(\phi)} \right)^2 \geq 1 \quad (\bar{\sigma}_{yy} > 0) \quad (4.22)$$

where $\bar{\sigma}_{yy}$ and $\bar{\sigma}_{xy}$ are the effective transverses and shear stress of the ply under consideration, respectively. $Y_t(\phi)$ is the effective ply transverse tensile strength. $S(\phi)$ is the effective ply shear strength. Expressions for $Y_t(\phi)$ and $S(\phi)$ are given in Reference [21].

Fiber-Matrix Shearing Failure

The failure criteria for the fiber-matrix shearing mode is a modified Hashin's criterion [33], and is as follows:

$$\left(\frac{\bar{\sigma}_{xx}}{X_t} \right)^2 + \left(\frac{\bar{\sigma}_{xy}}{S(\phi)} \right)^2 \geq 1 \quad (\bar{\sigma}_{xx} > 0) \quad (4.23)$$

When the matrix cracking failure or the fiber-matrix failure criteria is satisfied, the damage model increases the crack density ϕ by an amount $\Delta\phi$, and degrades the

material according to the failure mode. Then based on the current strain state and the newly degraded material properties, the model checks for further matrix cracking or fiber-matrix failure. This process of checking for failure and degrading the material when failure occurs continues until there is no further failure or when the crack density ϕ reaches the saturated crack density level ϕ_0 . Expressions for calculating ϕ_0 are given in Reference [21]. To simplify the modeling, this study keeps the crack density ϕ as an integer and sets $\Delta\phi$ as 1.

Chapter 5

Nonconvergence Problems

Predicting the fracture strength of composite laminate with cutouts using progressive failure analyses is difficult for two reasons. The first difficulty is in the damage modeling. The damage model must capture relevant damage mechanics so that accurate fracture strength prediction can be made. This is a difficult task and much work has been done in this area. The current study simply used a damage model that was recently developed by Shahid and Chang [21]. The second difficulty is on overcoming numerical problems in the finite element analyses brought on by the brittle nature of progressive failures in composites. The type of composites considered in this study are brittle materials. Thus, typical progressive damage models for these materials require highly discontinuous constitutive relations. These discontinuous material behaviors cause the numerical problems.

The focus of the current study is to overcome numerical problems in the finite element analyses. This chapter discusses numerical problems involved in performing composite progressive failure analyses. Since these numerical problems come from the constitutive relations defined by the material model, this chapter also discusses the damage model characteristics relating to these numerical problems.

5.1 Numerical Problems in Composite Progressive Failure Analysis

To determine the static fracture strength of a plate, a load is gradually applied to the plate until the final failure occurs. Although the applied load is quasi-static, the response of a notched composite plate loaded to ultimate failure will include both low rate events (quasi-static to structural dynamic rate regimes) and very high rate events (wave propagation rate regimes). The initial response will be in the quasi-static regime. When brittle failure occurs, discontinuous material behaviors will generate shocks in the plates, putting the plate response in a very high rate regime. Thus, the physics of these composite plate fracture problems have mixed response rate regimes.

The mixing of the response rates is not simple such as all low rate response initially and all high rate response after the first brittle failure occurs. In the real physical problem (laboratory tests), structural damping may damp out some shocks from initial failure. The damping may bring the plate response back to the low rate regime until more brittle failure occurs. When brittle failures do not lead to the ultimate structure failure, the plate is in a stable damage growth. In stable damage growths, the response rate may change arbitrarily.

The mixed response rates make analyses of composite progressive failure very difficult to do. Different solution procedures are used in finite element analyses to solve problems with different response rates [40-45]. Implicit solution procedures are more suited for problems involving low rate responses, and are normally used for quasi-static problems to structural dynamic problems. Explicit solution procedures are more suited for problems involving high speed dynamic events, and are used for wave propagation problems (shocks). It would be ideal to solve composite problems with mixed response rates by using an explicit procedure for high-rate response parts and an implicit procedure for low-rate response parts. However, because explicit and implicit solution procedures are very different [43], switching back and forth between these procedures is very difficult. Furthermore, the plate response rate in the composite fracture problems under consideration may change in a highly arbitrary and irregular manner. Thus, mixing implicit and explicit procedures may not be effective for these composite failure analyses.

It is possible to use an explicit solution procedure alone to perform the composite progressive failure analyses. However, there is a severe time-step restriction due to stability reasons for explicit solution procedures [41,43]. The very small time-step requirement due to this stability restriction, together with the type of quasi-static applied loading condition considered in the current study, would result in very costly and lengthy analyses. This makes explicit solution procedures impractical for slow rate events, which is a large part of the composite fracture problems under consideration.

Techniques such as mass scaling or velocity scaling may shorten analyses that uses an explicit procedure to model slow-speed events [40]. However, it is not clear if these techniques can be effective for the composite progressive analyses of concern.

Analyses that only use an implicit integration solution procedure alone will also be ineffective in solving the composite progressive failure problems of concern. Standard finite element codes use implicit procedures that are unconditionally stable with respect to time-step size [41]. Thus, implicit procedures can take step sizes that are orders of magnitude larger than step sizes required for explicit solution procedures. However, because implicit procedures require solutions of simultaneous equations and explicit procedures do not, each implicit time step costs orders of magnitude more than an explicit time step. Furthermore, because equilibrium is enforced at the end of a time step, analyses using implicit procedures for nonlinear problems require a nonlinear solution scheme that includes an interactive process along with convergence checks (e.g., the Newton-Raphson scheme) [43]. Thus, implicit solution procedures are effective if only a small number of time steps is needed. In the composite fracture problems under consideration, when brittle composite failure occurs, the rapidly changing

displacement field will require relatively very small time steps for convergence of the nonlinear solution scheme.

It is seen from laboratory experiments that, with respect to time, most of the response in these plate fracture tests is in the quasi-static regime. When brittle failure starts, shocks in stable damage growth are quickly damped out. Unstable damage growth or the final failure of these notched composite plates is instantaneous.

The current study chose to use the quasi-static solution procedure. Quasi-static solution procedures also use an implicit integration scheme, but do not include time dependent terms (inertia and viscous) in the equilibrium equation. Although, it is easier for an implicit dynamic procedure to converge than a quasi-static procedure in the nonlinear solution process, quasi-static procedures are much more efficient than the dynamic procedures for quasi-static loading problems.

The main difficulty in “implicit” analyses of composite fracture problems is the nonconvergence problems encountered in the nonlinear solution process. Equilibrium must be satisfied at each node within some given tolerance before a solution can be accepted. A nonconvergence problem occurs when the nonlinear solution scheme cannot find a displacement field that will satisfy equilibrium.

Quasi-static analyses do not include inertia and viscous forces, which are time dependent. Thus, these analyses can only capture solutions (displacement field) in static equilibrium states. When brittle failures cause shocks, the plate in the problem is in a dynamic equilibrium state. To continue these quasi-static analyses, the plate has to return to a static state from the dynamic state, and the nonlinear solution scheme must be able to find this static solution.

Displacement field “jumps” between two quasi-static solutions caused by brittle failure can be very large. Large displacement field change in a time increment means the solution at the end of that time increment is far from the solution at the beginning of the time increment. Thus, this results in difficult nonlinear problems. For “smooth” nonlinear problems, when a time increment is too large and the solution is changing too much, the analysis can cut down the increment size and begin again. With the smaller increment size, the solution at the end of the time increment will be closer to the solution at the beginning of the time increment. This makes it easier for the nonlinear solution scheme to find the solution. This time increment reduction technique will not work for brittle failures since the deformation will not be proportional to the load. Essentially, when a displacement jump occurs, quasi-static analyses must be able to find the next static solution, if one exists.

To illustrate a displacement jump, consider the example shown in Figure 5-1. In this example, a quasi-isotropic $[45/90/-45/0]_s$ unnotched plate is subjected to a uniaxial tension load in the 0° direction. Properties and parameters for the material T800/3900-2 (see Table 7-2) were used for all examples in this chapter. For the purpose of showing a displacement jump due to a sudden change in the plate stiffness, assume that the 45° plies have lower longitudinal tensile strength and that they will fail in the fiber breakage mode before the 0° ply will fail. When the 45° plies fail, they lose all of their stiffness and the residual stiffness of the laminate will be equivalent to a $[90/0]_s$ laminate. In a quasi-static analysis, when the 45° plies fail, the plate will adjust to the new stiffness and immediately jump to the static equilibrium displacement field. Figure 5-2 shows the history of the y displacement at the top of the plate. There is no static equilibrium during the jump. Thus, the nonlinear solution scheme must work hard to find the static equilibrium solution at the end of the jump.

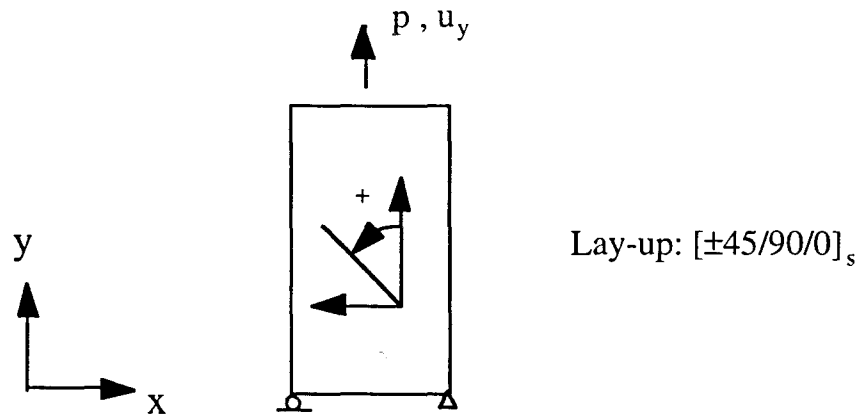


Figure 5-1. Example 5A: quasi-isotropic plate under uniaxial tension.

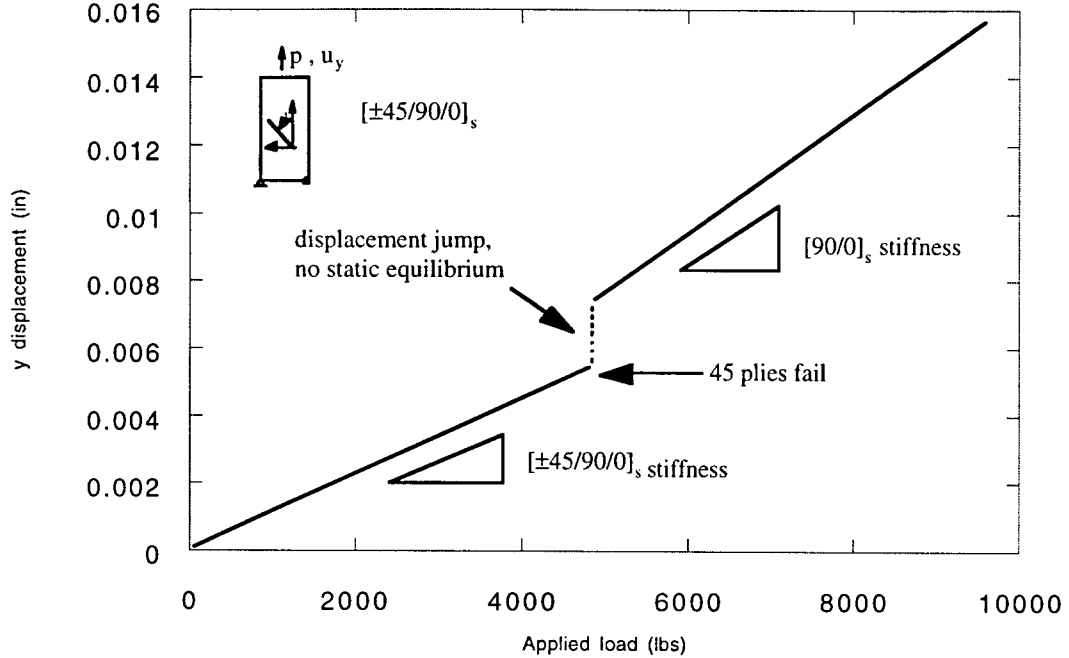


Figure 5-2. Displacement jump due to fiber failure in 45 plies.

5.2 Material Characteristics and Nonconvergence Problems

Brittle composite failures caused by abrupt stiffness losses generate shocks and put the plate response into high rate regimes. This section discusses characteristics of stiffness reductions due to the three failure modes included in the damage model selected for this study. The selected damage model described in Chapter 4 requires highly nonlinear material, constitutive relations, which is typical for composite progressive failure models. Of the three failure modes considered, the fiber failure modes causes sudden and total stiffness losses. The matrix cracking and fiber-matrix shearing failure modes cause only gradual stiffness losses.

Fiber tension failures are brittle failures. Equations 4.10 to 4.15 defined stiffness degradations due to the fiber tension failure mode. When the failure conditions are met, the material loses all of its stiffness immediately; the stiffness losses due to fiber failure are sudden and total. These abrupt stiffness losses will cause a singularity in the stress-strain relations. Essentially, all stiffnesses of the failed ply are removed. The effective stiffness of the laminate will be reduced abruptly, especially in the failed ply direction. If the effective laminate stiffness change is large, this stiffness change may generate shocks through the plate as it tries to readjust itself to the new stiffness and loading configuration. Thus, the material degradation from the fiber breakage failure mode will cause shocks and nonconvergence problems in the finite element analyses.

The matrix cracking failure mode causes only small and gradual stiffness losses. This failure mode is not a main cause of numerical problems. To illustrate matrix cracking stiffness degradations, consider Example 5A above again. In this example, the 90° plies are subjected to a transverse tensile load. Thus, these plies will fail in the matrix cracking mode. Figure 5-3 shows stiffness degradations in one of these 90° plies.

These degradations are typical matrix cracking degradations. Note that only Q_{xy} , Q_{yx} , and G_{xy} are reduced from the matrix cracking failure mode. These degradations are also more gradual compared to the stiffness losses in the fiber breakage failure mode. Q_{xx} , which is the fiber direction stiffness component, was not reduced by the matrix cracking failure mode. Fibers are the main load carrier in a unidirectional ply. Q_{xx} is about 20 times larger than the other stiffness components. Thus, the stiffness of the ply will not change significantly when matrix cracking failure occurs. Therefore, the laminate stiffness will also not change significantly. Matrix failure will not cause large change in the displacement field. Thus, matrix cracking failure only causes mild stiffness reductions, and therefore is not a concern in the task of overcoming nonconvergence problems.

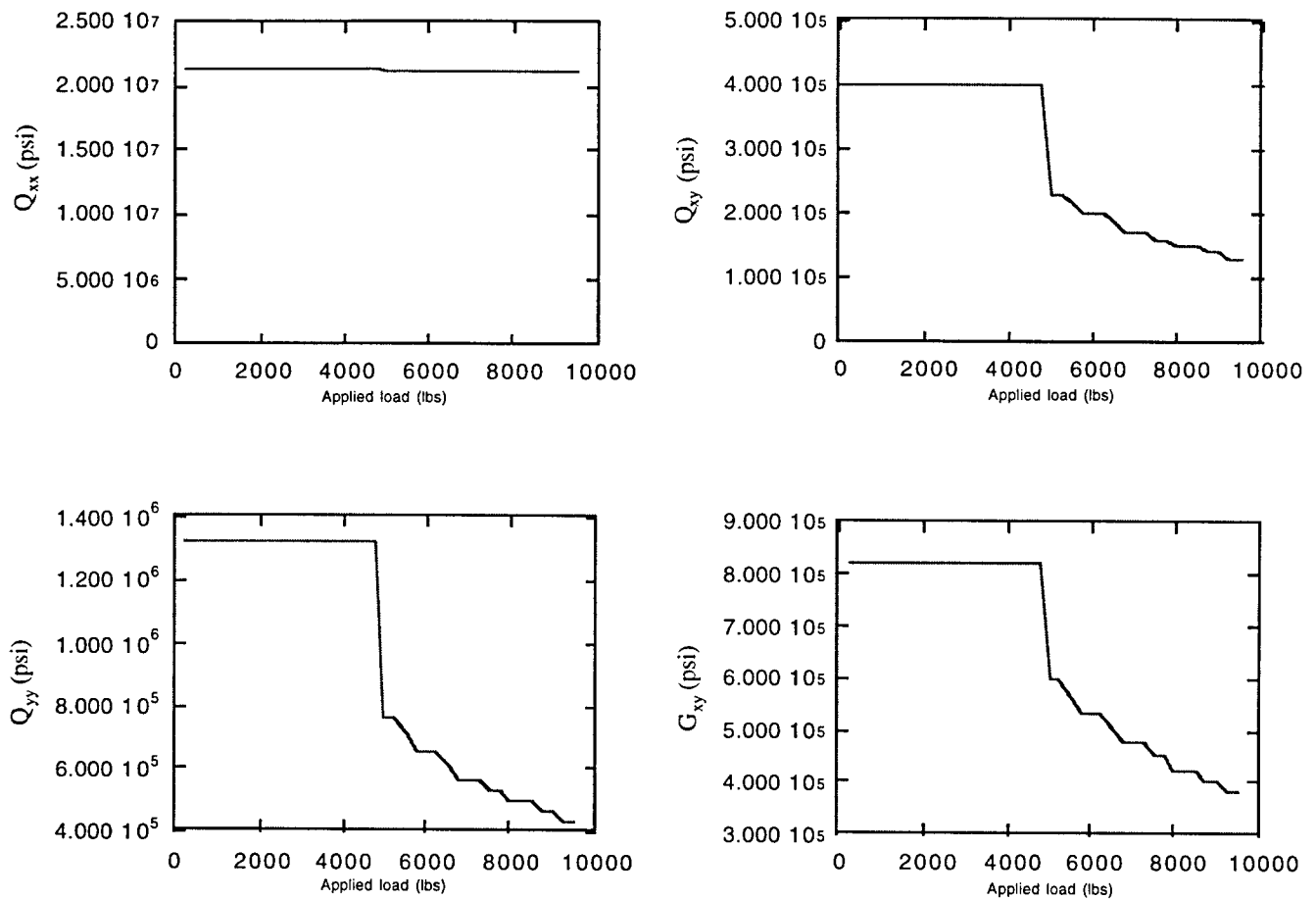


Figure 5-3. Stiffness degradations due to matrix cracking in 90° plies.

Similar to the matrix cracking failure mode, the fiber-matrix shear failure mode only causes gradual and mild stiffness reductions. Thus, this failure mode is also not a concern in the task of overcoming nonconvergence problems. Consider Example 5B shown in Figure 5-4. Here, a $[\pm 45]_s$ plate is subjected to a uniaxial tension load in the 0° direction. The plies will experience high shear stress, and fiber-matrix shear failure will occur. Figure 5-5 shows the stiffness degradations due to the fiber-matrix shear failure load in one of the 45 plies.

For the composite damage model developed by Shahid and Chang [21] and selected for this study, only the fiber breakage failure mode causes brittle material degradation that will cause dynamic instabilities. The matrix cracking and fiber-matrix shearing failure modes cause mild material degradations and are not the cause of numerical problems.

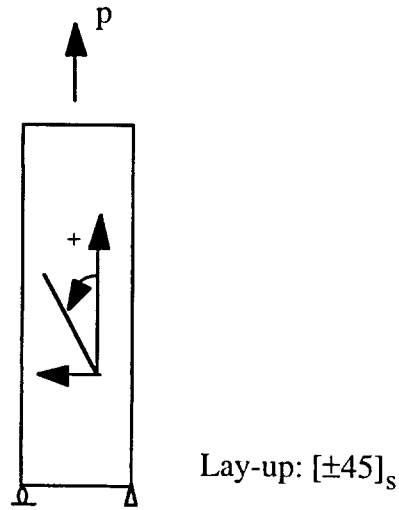


Figure 5-4. Example 5B: $[\pm 45]_s$ under uniaxial Tension

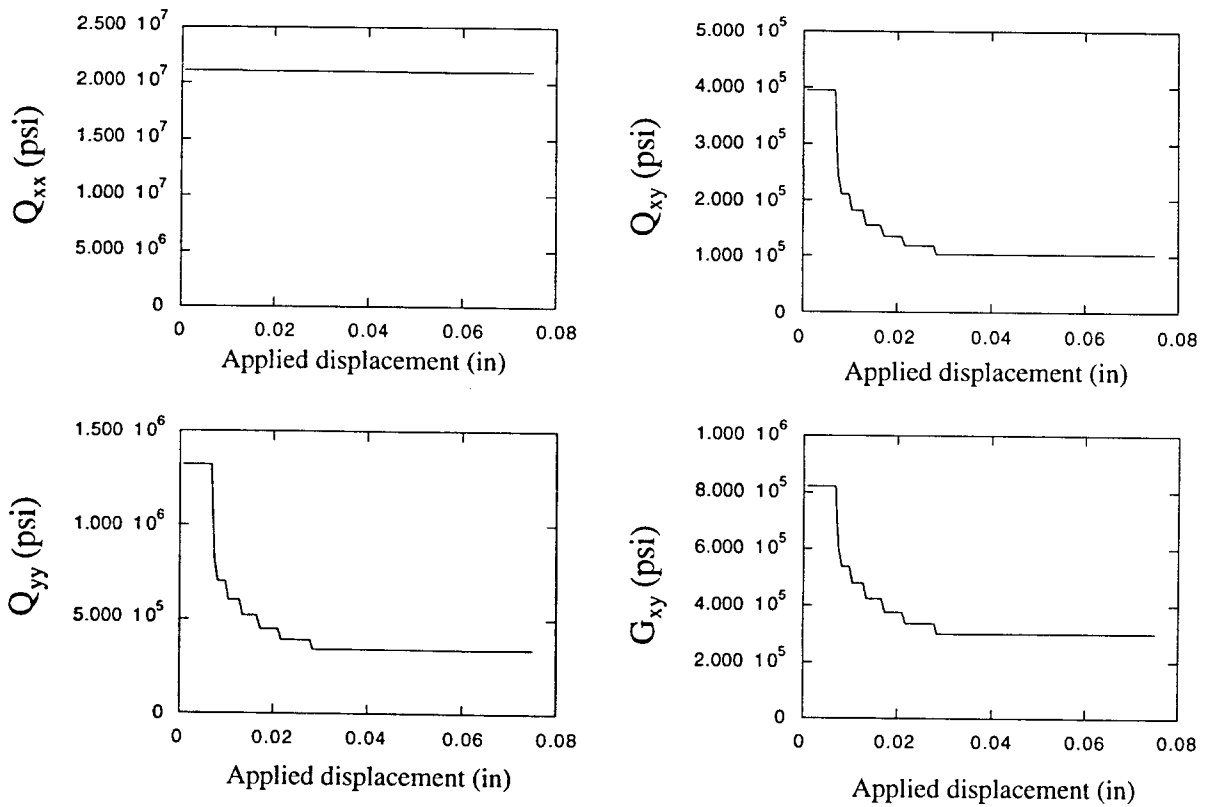


Figure 5-5. Stiffness degradations due to fiber-matrix shear failure are relatively gradual.

Chapter 6

Artificial Damping Model

To predict the fracture strength of notched composite plates, the current study uses finite element analyses along with a composite progressive damage model. The finite element analyses use a quasi-static solution procedure, which is an implicit integration scheme. Composite progressive failure analyses using quasi-static solution procedures will likely encounter nonconvergence problems as discussed in Chapter 5. This chapter presents treatments developed in this study to overcome these nonconvergence problems.

The nonconvergence problems arise from large and sudden deformations (shocks) due to brittle fiber failures. As discussed in Chapter 5, one way to model these shocks is to use an explicit integration scheme. However, this method would cost too much for the quasi-static loading problems under consideration. The approach taken in this study is to modify the material model so that the shocks will be suppressed and the analyses can be completed with just an implicit integration scheme.

Essentially, the current study opted to change very difficult problems involving both low and very high rate responses into easier problems with only low rate responses. This study assumes that for the purpose of predicting the plate fracture strength, it is not necessary to simulate the shocks. This assumption is critical, and must be verified on a case by case basis before the modeling method presented here can be successfully used.

6.1 Artificial Damping Model

To suppress the shocks in the analyses, this study added an artificial damping model to the damaged material model presented in Chapter 4. The artificial damping adds viscous stiffness to the material. This viscous stiffness acts as shock absorbers and suppresses shocks that may be caused by brittle fiber failures.

Damping is associated with a rate. There is no real time (as measured in seconds or minutes) in quasi-static analyses. However, nonlinear finite element analyses are solved incrementally with respect to the external load [38]. This external load can be parameterized by “time,” or equivalently, an external load parameter. In this study, the external load parameter, or the “time” in quasi-static analyses, is denoted by τ .

Let n denotes the increment number of the load step (n^{th} increment of the analysis). The time at the beginning of the increment n in the analysis is defined as:

$$\tau_n = \sum_{j=1}^{n-1} \Delta\tau_j \quad (6.1)$$

where $\Delta\tau_j$ is defined in this study as follows:

$$\Delta\tau_j = \frac{\Delta P_j}{P} \quad (6.2)$$

in which, P is the total external load to be applied, and ΔP_j is the magnitude of the external load applied in measure of the normalized external load progression.

Rate terms in these quasi-static analyses are defined in terms of τ . For example the longitudinal strain rate component for the increment n is calculate as:

$$\left(\dot{\bar{\epsilon}}_{xx}\right)_n = \frac{(\Delta\bar{\epsilon}_{xx})_n}{\Delta\tau_n} \quad (6.3)$$

Adding artificial damping to a material causes the stress in the material to be dependent on both the strain and the strain rate. Thus a stress surface replaces the stress-strain curve. In this study, the added artificial viscosity is only for overcoming nonconvergence problems, and not for modeling any physical behavior. Figure 6-1 shows a one-dimensional spring and dashpot representation of this model. Figure 6-2 shows the corresponding stress versus strain and strain rate surface for this one-dimensional model.

The purpose for adding the artificial damping model is to help the finite element analyses on overcoming nonconvergence problems. However, since the problem response is changed by the added artificial damping, this artificial damping may adversely change the fracture strength prediction. Thus, it is important to add the artificial damping such that it will overcome nonconvergence problems without significantly changing the plate fracture strength prediction. To do this, the current study tailored the artificial damping model for the characteristics of the selected composite progressive damage model.

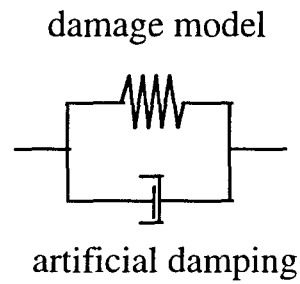


Figure 6-1. 1D spring and dashpot representation of the 1D model.

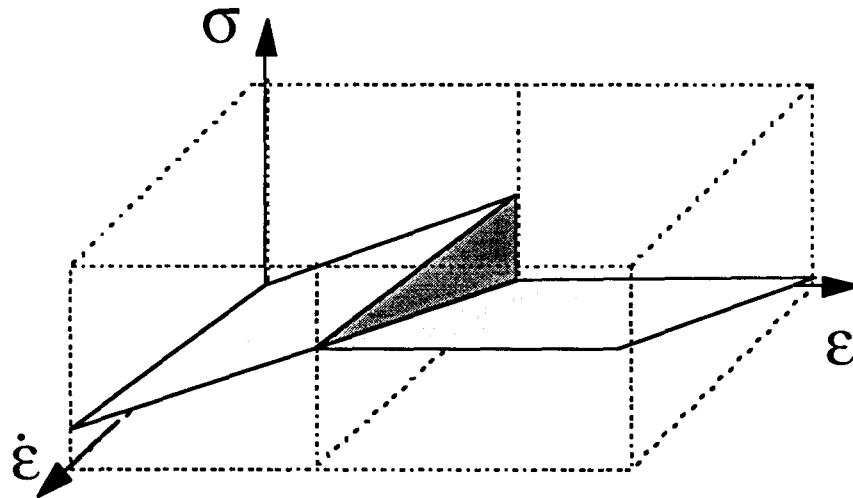


Figure 6-2. Stress surface of the 1D model.

The assumption that the added artificial damping will overcome the nonconvergence problems without significantly changing the final failure load prediction is absolutely critical to the success of the modeling with artificial damping method. If this assumption is accurate, the failure load prediction from the analysis can be used. If this assumption is not accurate, then this artificial damping is significantly changing the failure prediction. In this latter case, the failure load prediction should not be used.

Since the above assumption is so critical, it is also important to determine the effects of the artificial damping on the fracture strength prediction (the accuracy of the above assumption). This study uses multiple analyses at different levels of artificial damping (a parametric study) to do this. This study uses one active parameter in the artificial damping model to simplify required parametric studies.

The artificial damping is added by adding viscous stiffness in parallel to the elastic stiffness to the material model as depicted in Figure 6-1. Thus the stress in the material can be decomposed into an elastic part and an artificial damping part:

$$\sigma^{local} = \sigma_{elastic}^{local} + \sigma_{damping}^{local} \quad (6.4)$$

where σ^{local} denotes on-axis stress. $\sigma_{elastic}^{local}$ are defined by the composite damage model (Equations 4.1 and 4.2). The damping is artificial and should be tailored to overcome nonconvergence problems without significantly changing the failure load prediction. Based on the degradation characteristics of the selected composite damage model, the artificial damping is added to the composite as follows:

$$\sigma_{damping}^{local} = \begin{pmatrix} \bar{\sigma}_{xx} \\ \bar{\sigma}_{yy} \\ \bar{\gamma}_{xy} \end{pmatrix}_{damping} = \begin{pmatrix} b(s_f, \tau) \dot{\bar{\epsilon}}_{xx} \\ 0 \\ 0 \end{pmatrix} \quad (6.5)$$

where $b(s_f, \tau)$ is the artificial damping coefficient, τ is the analysis "time" previously defined. s_f is the state variable indicating whether fiber breakage failure has occurred or not. s_f is defined as follows:

$$s_f = 1 \quad \text{fiber failure occurred} \quad (6.6)$$

$$s_f = 0 \quad \text{no fiber failure} \quad (6.7)$$

Equation 6.5 can be written in terms of viscous stiffness as:

$$\begin{pmatrix} \bar{\sigma}_{xx} \\ \bar{\sigma}_{yy} \\ \bar{\gamma}_{xy} \end{pmatrix}_{damping} = \begin{pmatrix} b(s_f, \tau) & 0 & 0 \\ 0 & 0 & 0 \\ 0 & 0 & 0 \end{pmatrix} \begin{pmatrix} \dot{\bar{\epsilon}}_{xx} \\ \dot{\bar{\epsilon}}_{yy} \\ \dot{\bar{\gamma}}_{xy} \end{pmatrix} \quad (6.8)$$

The artificial damping coefficient is dependent on the damage state and the analysis time. The artificial damping is not added if failure has not occurred. $b(s_f, t)$ is defined as follows:

$$b(s_f = 0, \tau) = 0 \quad (6.9)$$

$$b(s_f = 1, \tau) = 0 \quad \tau < \tau_{ff} \quad (6.10)$$

$$b(s_f = 1, \tau) = b_0 \quad \tau_{ff} < \tau \leq (\tau_{ff} + \tau_v) \quad (6.11)$$

$$b(s_f = 1, \tau) = b_0 \left(1 - \frac{(\tau - \tau_{ff} - \tau_v)}{\tau_r} \right) \quad (\tau_{ff} + \tau_v) < \tau < (\tau_{ff} + \tau_v + \tau_r) \quad (6.12)$$

$$b(s_f = 1, \tau) = 0 \quad (\tau_{ff} + \tau_v + \tau_r) < \tau \quad (6.13)$$

where b_0 is the initial damping coefficient, τ_{ff} is the fiber failure time, and τ_v is the initial period of full damping, and τ_r is the damping ramp down period. b_0 , τ_v , and τ_r are parameters required for the viscous model. However, this study use constants τ_v and τ_r that the viscous model is essentially a simple one active parameter model. The artificial damping distribution in Figure 6-3.

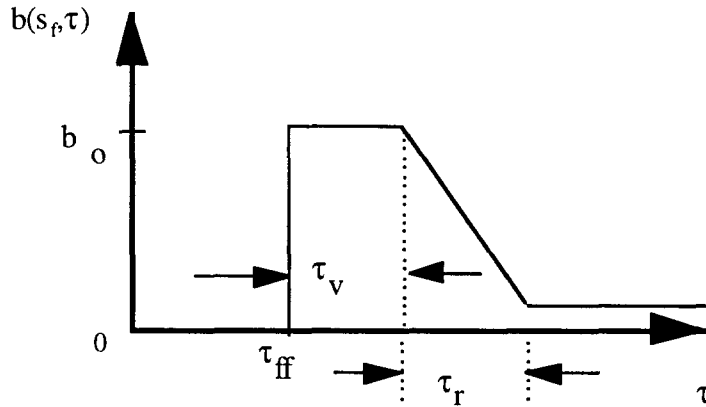


Figure 6-3. Artificial damping distribution.

In Equation 6.8, only the damping component in the fiber direction of the ply is new. This damping coefficient is a function of the damage state and the analysis time. Here is how the model attempts to add artificial damping only where and when it is needed. The model only adds artificial damping after the fiber failure mode is detected. Fiber failure causes the shocks, which cause nonconvergence problems. Without brittle fiber failures, there would be no shocks, and there would be no need for artificial damping. The model adds damping only in the fiber direction, because most of the load in the other direction is carried by other plies, not by the ply that has just failed. The model removes damping after a predetermined period τ_v . Also there is no need for artificial damping anymore once convergence is attained. Thus, the damping is

removed slowly(ramped down linearly) over a predetermined period τ_r after fiber failure occurs.

The familiar stress resultant to strain relations for symmetric composite laminates subjected to only in-plane load [24,26] are:

$$\mathbf{N} = \mathbf{A}\boldsymbol{\varepsilon}^o \quad (6.14)$$

where \mathbf{N} is the in-plane stress resultant force (integration of stress through the thickness) of the plate. \mathbf{A} is the plate extensional stiffness. $\boldsymbol{\varepsilon}^o$ is the plate extensional strain. With the artificial damping, Equation 6.14 becomes:

$$\mathbf{N} = \mathbf{A}\boldsymbol{\varepsilon}^o + \mathbf{A}'\dot{\boldsymbol{\varepsilon}}^o \quad (6.15)$$

where \mathbf{A}' is the extensional viscous stiffness of the plate and $\dot{\boldsymbol{\varepsilon}}^o$ is the extensional strain rate (defined in terms of $\Delta\tau$). Appendix A gives more details on these relations including the characteristics of \mathbf{A}' . Note that the viscous terms come from the artificial damping, which is added only to overcome nonconvergence problems. The viscous terms are not real material behavior, and should be included only as part of the incremental solution process.

6.2 Modeling Strategy

The validity of this modeling with artificial methods depend on the accuracy of the above assumption. The accuracy of this assumption varies from problem to problem. There is no prior knowledge of this assumption accuracy. However, this accuracy may be determined by using multiple analyses for the same problem at different levels of artificial damping (a parametric study),

In ideal problems, the parametric study will show that the above assumption is accurate, and the failure load prediction can be confidently used. In troublesome problems, the parametric study will show that the above assumption is inaccurate, and this modeling method can not be used. Figure 6-4 shows a typical failure load prediction versus artificial damping plot that may be generated from a parametric study.

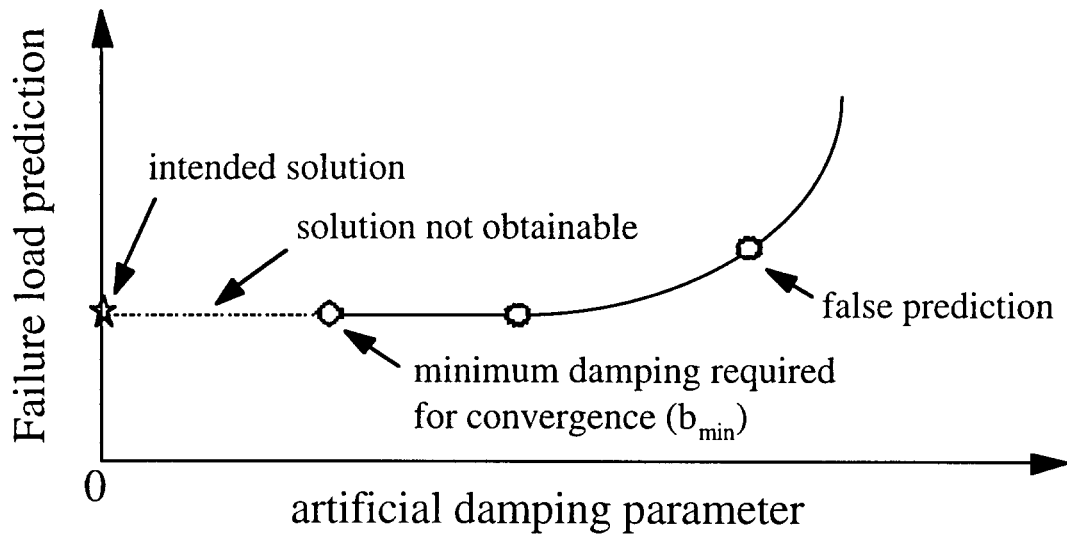


Figure 6-4. Typical damping effects on failure load prediction.

The plot in Figure 6-4 shows effects of the artificial damping on the failure load prediction. The accuracy of the assumption that the damping does not have significant effects on the failure load prediction can be determined from such a plot. The beginning part of this plot is expected to be flat. The elastic stiffness (damage model component) and the damping stiffness are in parallel. Thus, when the damping stiffness is very low relative to the damage stiffness, the material behavior is dominated by the damage model, and the artificial damping will not have significant effects on the failure load prediction. At zero damping, the material is just the damage model. Failure load prediction at zero damping is the intended solution, which is what the damage plus damping model tries to obtain. On the opposite end, when the damping level and thus the damping stiffness is relatively high compared to the elastic stiffness, the material behavior is dominated by the damping. In these cases, the artificial damping will have significant effects on the failure load prediction.

Thus, if the failure load prediction is on the initial flat part of the curve, the main assumption is accurate, and the prediction can be used. If the failure load prediction is not on the initial flat part of the curve, the main assumption is not accurate, and the prediction cannot be confidently used. A few points on this plot that are far enough from each other can determine whether a prediction is on this flat part of the curve. And so, a parametric study is required to assess the accuracy of the all important main assumption.

For analyses with nonconvergence problems, failure prediction on the first part of the curve will not be obtainable due to nonconvergence problems. This is the reason for the current research. In these problems, there will be a minimum amount of artificial

damping level, b_{\min} , that must be used to overcome all nonconvergence problems so that a failure load prediction can be made. Ideally, all higher artificial damping levels will overcome all nonconvergence problems and yield a failure load prediction. Based on the monotonical nature of Figure 6-4, the best failure load prediction using the artificial damping modeling method is at the b_{\min} artificial damping level. Thus, it is important to obtain a failure prediction using b_{\min} or a little higher value of artificial damping, and also to determine where this failure prediction is on the failure load versus artificial damping curve.

With only one active damping parameter, the artificial damping model makes it easy to perform the required parametric study and to estimate b_{\min} . With just one active parameter, each analysis provides a point on the failure load versus artificial damping curve. The current study uses a simple algorithm to estimate b_{\min} automatically from the first analysis as follows. The first analysis is started with zero artificial damping. Convergence characteristics are monitored throughout the analysis. When nonconvergence problems are detected, the material model increases the artificial damping level by small increments, and this level of artificial damping is used from then on. The process continues until the end of the analysis. The maximum level of artificial damping used in the first analysis is the estimated b_{\min} .

With b_{\min} estimated from the first analysis, the parametric study can be performed by simply increasing the level of artificial damping based on the estimated b_{\min} . In ideal problems, order of magnitude changes in the artificial damping level will not cause significant changes in the failure load prediction.

The developed damping model is easy to implement and use. It has one active parameter. This parameter is estimated during the finite element analysis run. The active model parameter, the damping level, is not a parameter to calibrate the failure prediction of the model. In fact, the key assumption, which is required for the artificial damping model, is accurate only when this damping level has little or no effect on the failure load prediction.

6.3 Material Model Implementation

The current modeling method uses finite element analyses by ABAQUS/Standard (referred from here on simply as ABAQUS) and the developed damage model to predict the tension fracture strength of notched composites. The damage model interacts with ABAQUS through a user defined material subroutine [34-37]

All analyses performed in this study were quasi-static. These analyses used the finite deformation theory [35,38] to model the large deformation expected from composite brittle failures.

This study uses layered shells to model the composite laminates [36]. The laminate layups, the plies' thicknesses and orientations are input directly into ABAQUS. With these input, ABAQUS performed the stiffness transformations of the layers and the stiffness integration through the thickness of the laminates outside of the material user subroutine. Thus, the subroutine only needs to define the on-axis material behavior [35]. In addition, ABAQUS also performed the transformations of the stresses and strains due to rigid body rotation for finite deformation theory outside of the material user subroutine. Thus, the material subroutine defines the material behavior in terms of Cauchy Stress and logarithmic strain [34,35,39].

ABAQUS calls the material subroutine for each material calculation point at each iteration of every increment. When the subroutine is called, ABAQUS passes in the material state at the start of the increment (stress, solution dependent state variables, etc.), the strain increments, and the time increment. The subroutine calculates the stress and the solution dependent state variables at the end of the increment and also the material Jacobian matrix $\frac{\partial \bar{\sigma}^{local}}{\partial \bar{\epsilon}^{local}}$ for the current increment [34]. The material Jacobian is defined as:

$$\frac{\partial \bar{\sigma}^{local}}{\partial \bar{\epsilon}^{local}} = \begin{pmatrix} \frac{\partial \bar{\sigma}_{xx}}{\partial \bar{\epsilon}_{xx}} & \frac{\partial \bar{\sigma}_{xx}}{\partial \bar{\epsilon}_{yy}} & \frac{\partial \bar{\sigma}_{xx}}{\partial \bar{\gamma}_{xy}} \\ \frac{\partial \bar{\sigma}_{yy}}{\partial \bar{\epsilon}_{xx}} & \frac{\partial \bar{\sigma}_{yy}}{\partial \bar{\epsilon}_{yy}} & \frac{\partial \bar{\sigma}_{yy}}{\partial \bar{\gamma}_{xy}} \\ \frac{\partial \bar{\sigma}_{xy}}{\partial \bar{\epsilon}_{xx}} & \frac{\partial \bar{\sigma}_{xy}}{\partial \bar{\epsilon}_{yy}} & \frac{\partial \bar{\sigma}_{xy}}{\partial \bar{\gamma}_{xy}} \end{pmatrix} \quad (6.16)$$

Equation 6.16 required by ABAQUS is the "tangent stiffness" of the material stress-strain curve. The "tangent stiffness" works well for smooth nonlinear material behavior such as metal plasticity. However, for brittle material behavior, where the stress-strain curve contains discontinuities (drops), methods using "tangent stiffness" will have problems. This study uses a "secant stiffness" method to model composite brittle material behavior. The secant method calculates the stress from total strain with updated (damaged) stiffness.

Figure 6-5 illustrates the nonlinear solution method using “secant stiffness”. This nonlinear example problem will be solved by breaking the displacement controlled external load, d , into small increments. The solution is solved incrementally using iterations inside the increments when a nonlinearity (failure) occurs. This method uses the current stiffness, and the total strain to calculate the current stress. When failure is detected by the failure criteria in the model, a new, reduced stiffness is calculated.

Let the subscript n denotes the increment counter, and the superscript k denotes the iteration counter inside the n^{th} increment. The nonlinear solution scheme works for an increment n that contains 1 failure as follows. The increment start with the load P_n^0 and the displacement d_n . The first iteration uses the stiffness at the start of the increment, Q_a . From this stiffness and he applied displacement d_{n+1} , the load P_n^1 is obtained. This load will satisfy the failure criteria ($d > d_f$), which will prompt the solution scheme to degrade the stiffness to Q_b , and start the second iteration. From the applied displacement d_{n+1} and the new stiffness Q_b , the new load P_n^2 is calculated. With this load, no more failure is predicted and this load becomes the solution for increment n .

The solution at any point in this problem is linear. The solver can obtain this solution in 1 calculation if the correct (degraded) stiffness is used. Thus, in the above example, 1 extra iteration was required to account for 1 failure (1 stiffness change). The selected damage material model defines the material as elastic with damage. Thus, this study uses the “secant stiffness” for these problems.

The functions of the material model in an ABAQUS analysis are to defined the on-axis stress $\bar{\sigma}^{local}$ the solution dependent state variables (damage state of the material) at the end of

the current increment, and the on-axis Jacobian matrix $\frac{\partial \bar{\sigma}^{local}}{\partial \bar{\epsilon}^{local}}$ for the layer under consideration.

The material model uses Equation 6.4 to calculate the total stress to be returned to ABAQUS. Chapter 4 presented the equations for calculating the elastic stress $\bar{\sigma}_{elastic}^{local}$ and the solution dependent state variables. The model uses Equation 6.8 to calculate the damping stress $\bar{\sigma}_{damping}^{local}$. Combining these equations, the component of the total stress to be returned to ABAQUS are:

$$\bar{\sigma}_{xx} = Q_{xx}^D \bar{\epsilon}_{xx} + Q_{xy}^D \bar{\epsilon}_{yy} + b(s_f, \tau) \dot{\bar{\epsilon}}_{xx} \quad (6.17)$$

$$\bar{\sigma}_{yy} = Q_{xy}^D \bar{\epsilon}_{xx} + Q_{yy}^D \bar{\epsilon}_{yy} \quad (6.18)$$

$$\bar{\gamma}_{xy} = \frac{\bar{\sigma}_{xy}}{G_{xy}^D} + \alpha \left(\frac{\bar{\sigma}_{xy}}{G_{xy}^D} \right)^3 \quad (6.19)$$

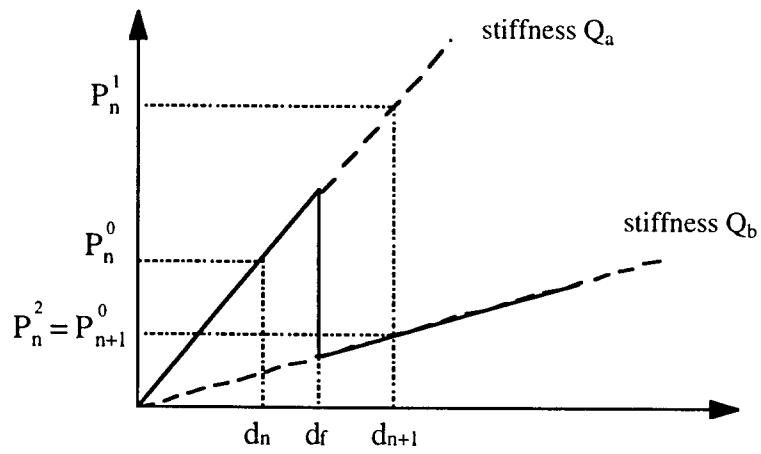
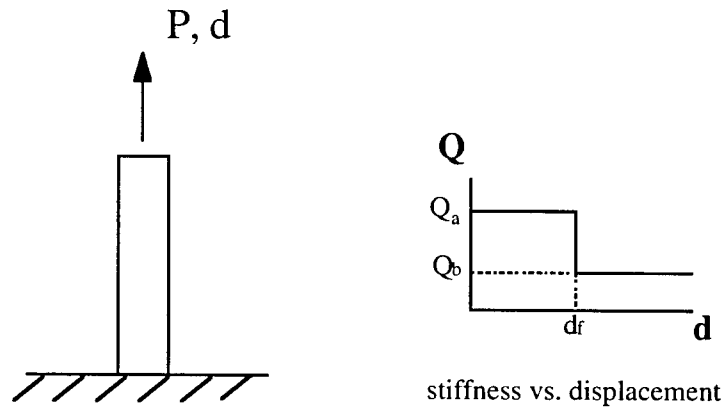


Figure 6-5. Secant method to model brittle failure.

The constitutive relations for $\bar{\sigma}_{yy}$ and $\bar{\gamma}_{xy}$ are elastic and rate independent. Thus, the Jacobian components relating to these stress are just the elastic stiffness:

$$\frac{\partial \bar{\sigma}_{yy}}{\partial \bar{\epsilon}_{xx}} = Q_{yx}^D \quad (6.20)$$

$$\frac{\partial \bar{\sigma}_{yy}}{\partial \bar{\epsilon}_{yy}} = Q_{yy}^D \quad (6.21)$$

$$\frac{\partial \bar{\sigma}_{yy}}{\partial \bar{\gamma}_{xy}} = 0 \quad (6.22)$$

$$\frac{\partial \bar{\sigma}_{xy}}{\partial \bar{\epsilon}_{xx}} = 0 \quad (6.23)$$

$$\frac{\partial \bar{\sigma}_{xy}}{\partial \bar{\epsilon}_{yy}} = 0 \quad (6.24)$$

$$\frac{\partial \bar{\sigma}_{xy}}{\partial \bar{\gamma}_{xy}} = \frac{1}{G_{xy}^D + \frac{3\alpha(\bar{\sigma}_{xy}\bar{\sigma}_{xy})}{(G_{xy}^D)^3}} \quad (6.25)$$

The calculations of the $\frac{\partial \bar{\sigma}^{local}}{\partial \bar{\epsilon}^{local}}$ components for $\bar{\sigma}_{xx}$ use

the stable central difference operator [34]:

$$\dot{f}_{\tau+\frac{\Delta f}{\Delta \tau}} = \frac{\Delta f}{\Delta \tau} \quad (6.26)$$

$$f_{\tau+\frac{\Delta \tau}{2}} = f_{\tau} + \frac{\Delta f}{2} \quad (6.27)$$

where f is some function, f_{τ} is its value at the beginning of the increment, Δf is the change in the function over the increment, and $\Delta \tau$ is the time increment. Applying this to Equation 6.17 for the $\tau + \frac{\Delta \tau}{2}$ gives:

$$(\bar{\sigma}_{xx})_{\tau} + \frac{\Delta \bar{\sigma}_{xx}}{2} = Q_{xx}^D \left((\bar{\epsilon}_{xx})_{\tau} + \frac{\Delta \bar{\epsilon}_{xx}}{2} \right) + Q_{xy}^D \left((\bar{\epsilon}_{yy})_{\tau} + \frac{\Delta \bar{\epsilon}_{yy}}{2} \right) + b(s_f, \tau) \frac{\Delta \bar{\epsilon}_{xx}}{\Delta \tau} \quad (6.28)$$

The components related to $\bar{\sigma}_{xx}$ are calculated as $\frac{\partial(\Delta \bar{\sigma}_{xx})}{\partial(\Delta \bar{\epsilon}_{ij})}$ in Equation 6.28:

$$\frac{\partial \bar{\sigma}_{xx}}{\partial \bar{\epsilon}_{xx}} = Q_{xx}^D + \frac{2b(s_f, \tau)}{\Delta \tau} \quad (6.29)$$

$$\frac{\partial \bar{\sigma}_{xx}}{\partial \bar{\epsilon}_{yy}} = Q_{xy}^D \quad (6.30)$$

$$\frac{\partial \bar{\sigma}_{xx}}{\partial \bar{\gamma}_{yy}} = 0 \quad (6.31)$$

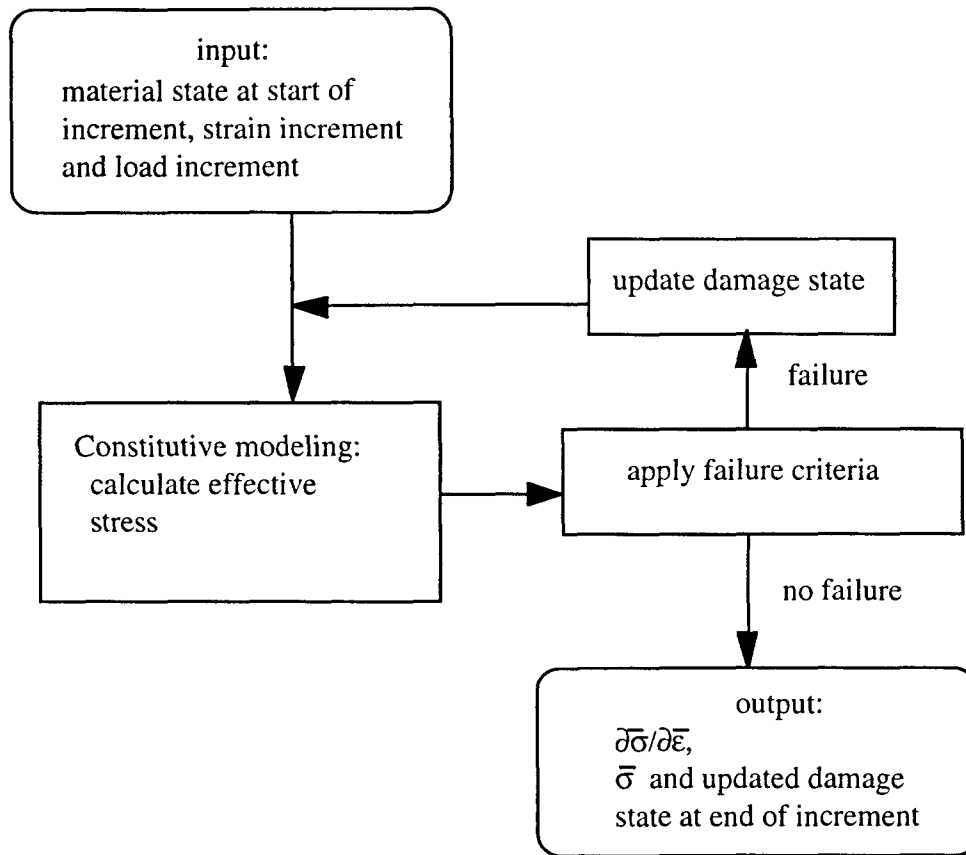


Figure 6-6. Flow chart of material model subroutine.

Chapter 7

Model Verification

The developed composite progressive failure model was verified using two sets of experimental data. The first set included small coupons with simple geometry under uniaxial tension load. The second set included large panels with more complex geometry under both uniaxial tension and biaxial tension load. This chapter presents the verification cases, the finite element analyses, failure load comparisons between experimental data and model predictions, and the effects of the artificial damping on failure load predictions.

Without the artificial damping component, finite element analyses using the developed damage model alone represent old, existing modeling methods. The focus of this research was to overcome nonconvergence problems often encountered when using these existing modeling methods. Thus, analyses using the damage model with the developed artificial damping model represent new modeling methods for predicting the composite fracture strength developed in this research. This chapter compared the composite plate fracture strength predictions between the old and new modeling methods.

7.1 Small Coupon Verification

The objective of the small coupon tests was to verify both the existing modeling methods (analyses with damage model alone) and the new modeling method (analyses with both the damage model and the artificial damping model) for the simple geometry. Since the geometry was simple, both modeling methods were expected to perform reasonably well.

Experimental Data

The experimental data for the small coupon tests was obtained from Sandia National Laboratories [50]. There were nine test cases that included five coupon geometries, one material, three lay-ups, and one loading. Figure 7-1 shows the basic test configuration. Figure 7-2 shows the five geometries. The material was Toray 3900-2. Table 7-1 summarizes the data of the nine small coupon test cases.

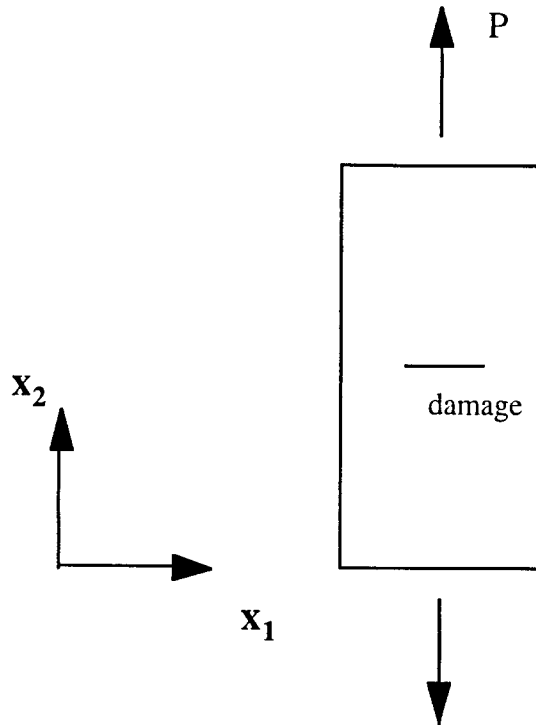


Figure 7-1 Small coupon test configuration.

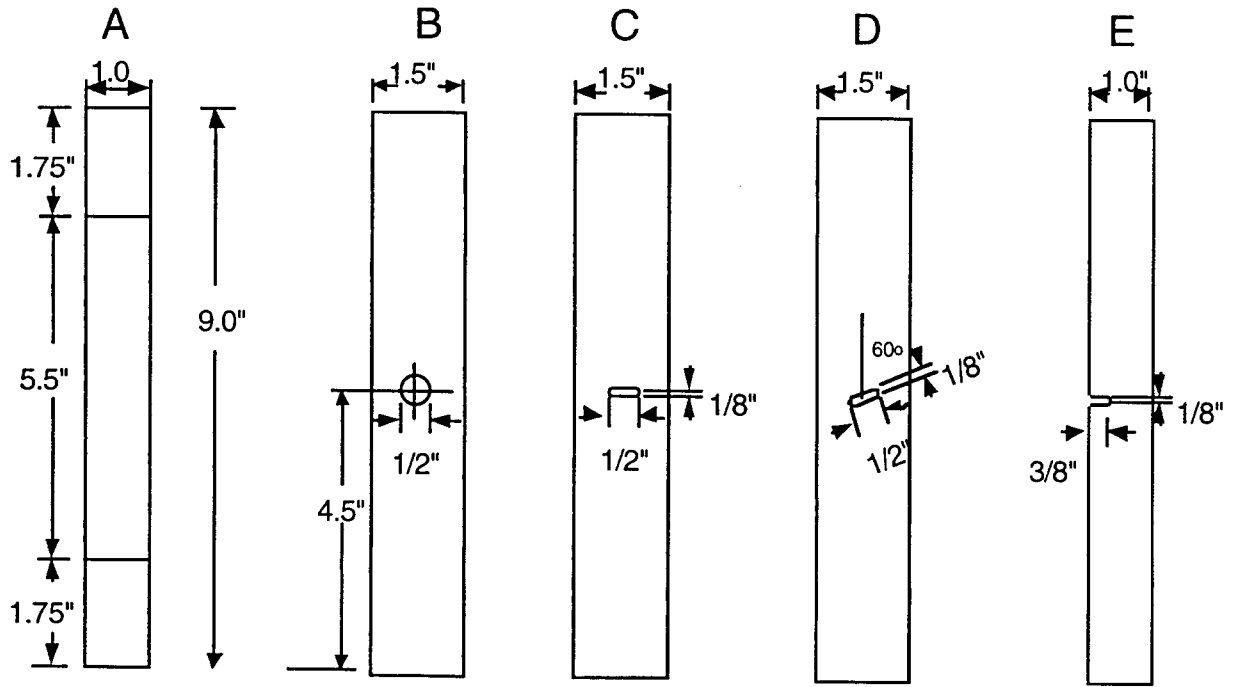


Figure 7-2 Small coupon test geometries.

Table 7-1. Small coupon test cases.

| Case | Geometry | Material | Lay-up | |
|------|----------|----------|-----------------|---|
| 70A | S | A | T800/3 900-2 | $[(45/90/-45/0)_2]_s$ |
| 70B | S | B | T800/3 900-2 | $[(45/90/-45/0)_2]_s$ |
| 76B | S | B | T800/3 900-2 | $[45/90/-45/0/ \mp 45/90 \pm 45/0/ \mp 45]_s$ |
| 70C | S | C | T800/3 900-2 | $[(45/90/-45/0)_2]_s$ |
| 70D | S | D | T800/3 900-2 | $[(45/90/-45/0)_2]_s$ |
| 54D | S | D | T800/3 900-2 | $[-45/0/45/90_2/-45/90_2/45/0]_s$ |
| 76D | S | D | T800/3 900-2 | $[45/90/-45/0/ \mp 45/90 \pm 45/0 \pm 45]_s$ |
| 70E | S | E | T800/3 900-2 | $[(45/90/-45/0)_2]_s$ |
| 54E | S | E | T800/3 900-2 | $[-45/0/45/90_2/-45/90_2/45/0]_s$ |

Progressive Damage Analysis

All analyses in this study were quasi-static analyses. Since large deformation was expected due to the brittle nature of composite failures, the analyses used finite deformation theory [35, 38,39].

Finite element analyses using the damage model alone and the combination of the damage model and the artificial damping model were performed for the nine small coupon test cases. This study used the commercial finite element code ABAQUS/Standard to perform the element analyses. The analyses used an implicit

integration scheme, a quasi-static solution procedure. The reduced integration S4R shell element in ABAQUS was selected for this study.

The uniaxial tension load was applied by prescribing displacement controlled boundary conditions. The x_2 displacement was fixed at the bottom side of the coupon. The load was applied by prescribing a x_2 displacement at the top side. Figure 7-3 shows the loading and boundary conditions of small coupon analyses. In simplifying the analyses, only half of coupon geometry B and C were modeled. This study assumed that the deformation and damage growth were symmetric about the $x_2 - x_3$ plane.

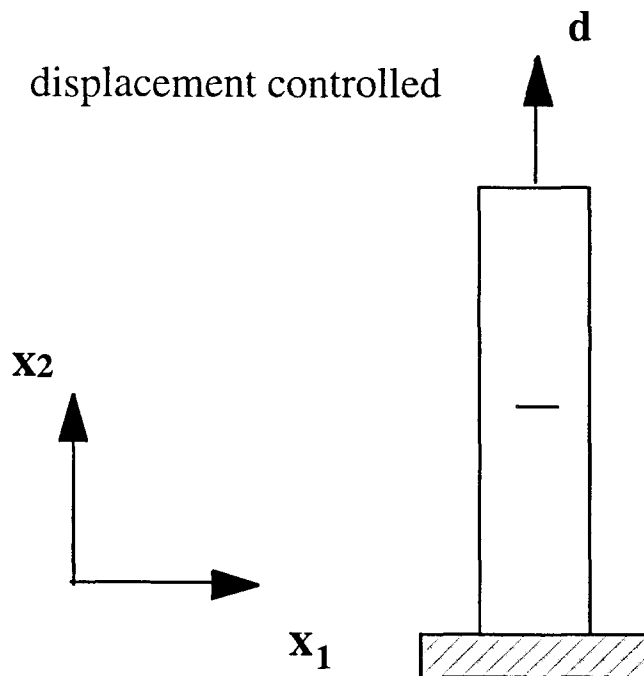


Figure 7-3. Boundary condition and displacement controlled load condition.

The composite laminates were modeled using layered shell elements. Each layer represented a ply, and each ply had its own principal orientation. The analyses used three- and sometimes five-section integration points for each layer [36]. Table 7-2 shows the material properties and the damage model parameters used for the Toray 3900-2 graphite/epoxy system.

The finite element meshes for coupon geometries B, C, D, and are shown in Figure 7-4.

Table 7-2. Properties and parameters used in small coupon analyses.

| Properties | T800/3900-2 |
|--------------------------------|-------------|
| E_x (msi) | 23.2 |
| E_y (msi) | 1.30 |
| ν_{xy} | 0.28 |
| G_{xy} (msi) | 0.90 |
| α (1/psi ³) | 1.0e-14 |
| G_{yz} (msi) | 0.50 |
| G_{xz} (msi) | 0.90 |
| <u>Thermal</u> | |
| α_x (1/F) | 0.22e-6 |
| α_y (1/F) | 16.03-6 |
| T_{cure} (F) | 340 |
| T_{room} (F) | 75 |
| <u>Other</u> | |
| <u>Properties</u> | |
| | 412 |
| X_t (ksi) | |
| δ (in.) | 0.041 |
| h (in.) | 0.0065 |
| G_{lc} (lb/in.) | 1.65 |
| G_{llc} (lb/in.) | 3.30 |
| τ_v | 0.03 |
| τ_r | 0.05 |

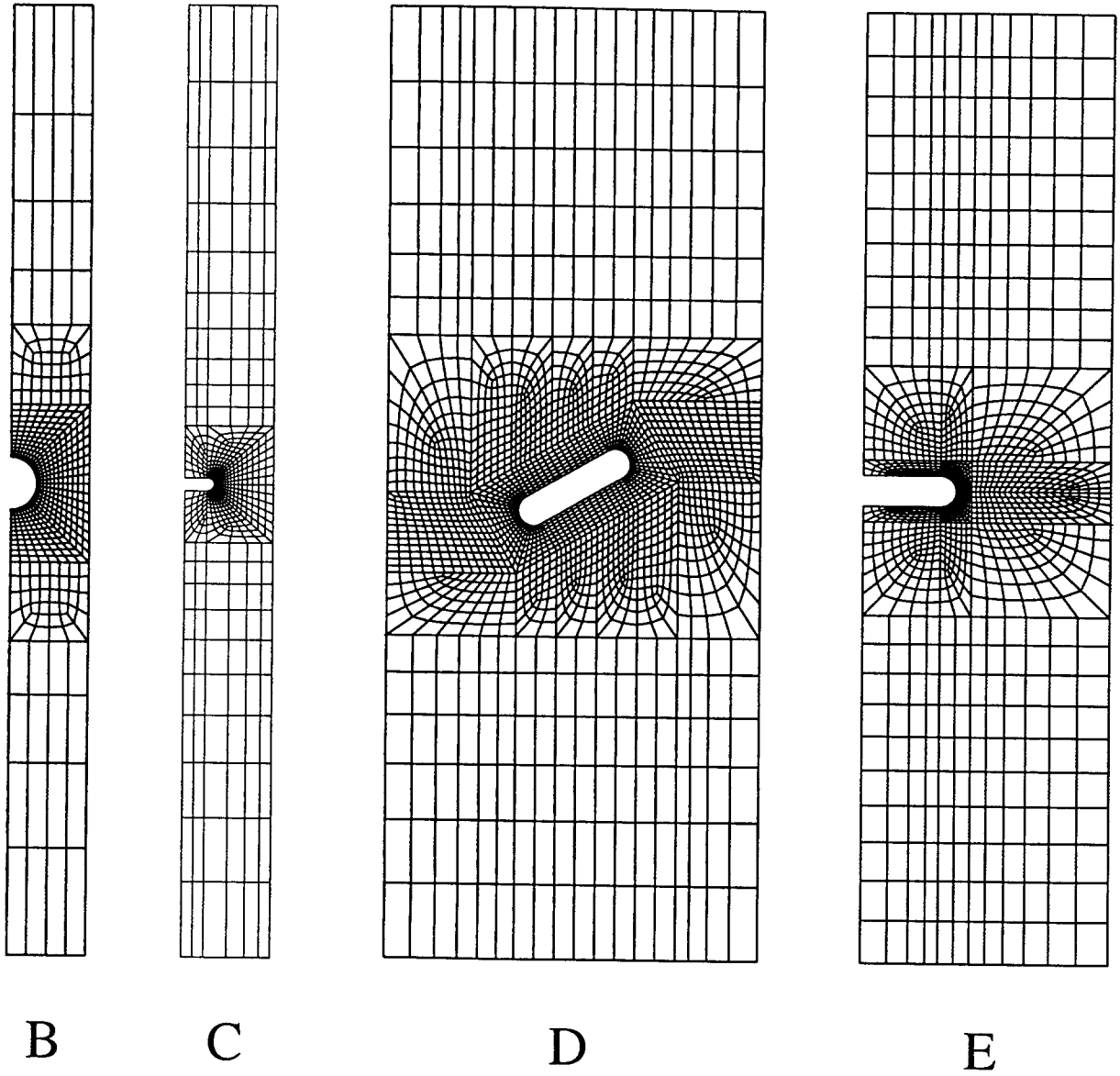


Figure 7-4. Finite element meshes for small coupon analyses (not to scale).

Failure Load Comparison

Table 7-3 summarizes failure load results for the small coupons. Figure 7-5 plots the two predictions normalized by the experimental data. Predictions using both the damage model and the damping model represented new capability from this study. Predictions using the damage model alone represent an existing modeling method.

Table 7-3. Failure load comparison for small coupons.

| Case | Test data (lb) | Damage/Da mping (lb) | Damage (lb) |
|------|-------------------|----------------------------|----------------|
| S70A | 15,700 | 16,290 | 16,290 π |
| S70B | 10,200 | 10,600 | 10,600 |
| S76B | 11,300 | 12,800 | 12,800 |
| S70C | 9,900 | 10,600 | 10,500 |
| S70D | 9,900 | 9,420 | 9,420 |
| S54D | 8,300 | 8,220 | 8,200 |
| S70D | 5,800 | 6,100 | 5,700 |
| S54E | 3,100 | 3,700 | 3,500 |
| S76E | 5,800 | 6,100 | 5,700 |

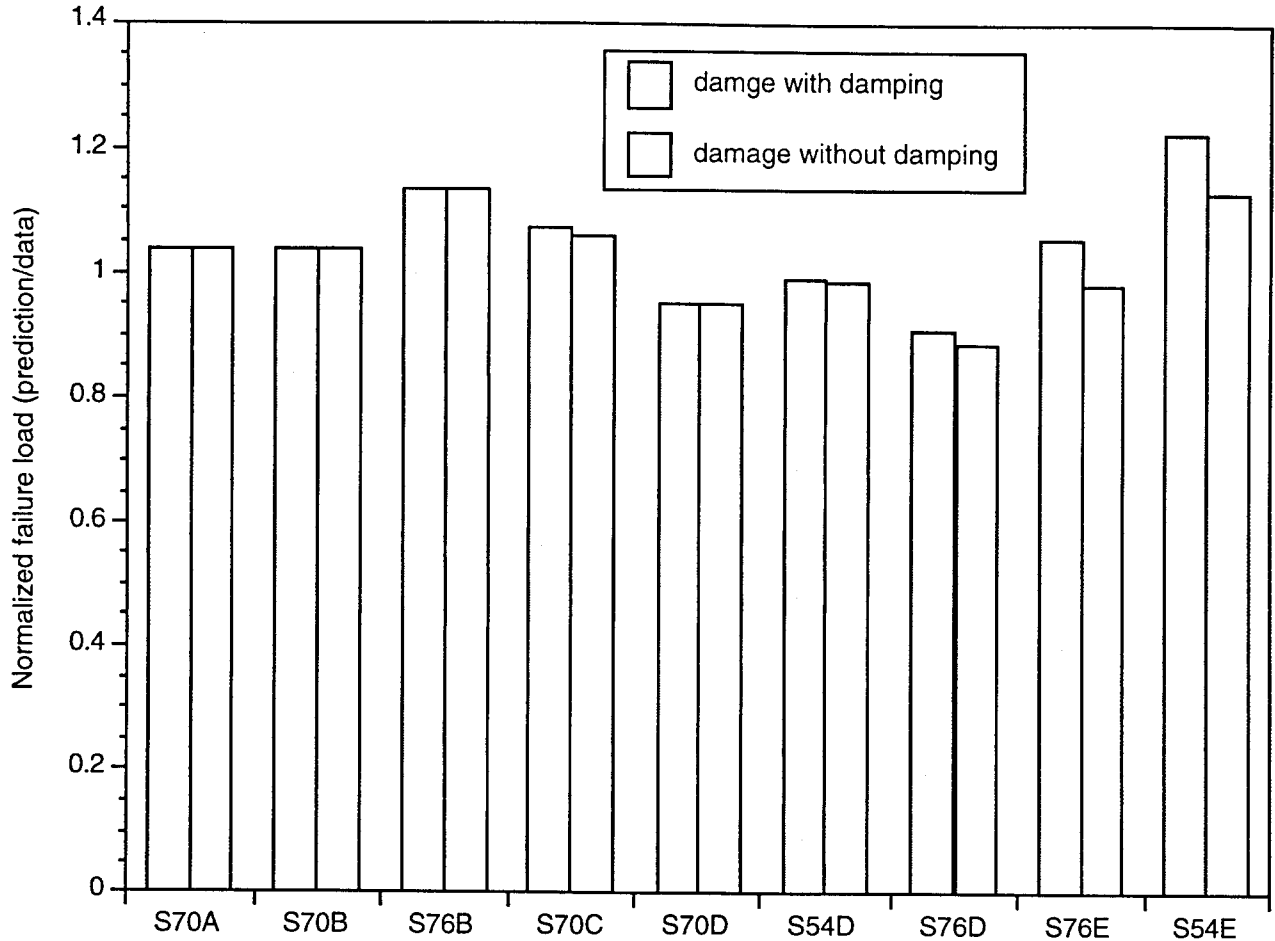


Figure 7-5. Fracture strength comparison for small coupons.

These results show that the damage with damping model predicted failure load of large panels with more complex geometry reasonably well. Without the artificial damping, the damage model alone could not have overcome nonconvergence problems and terminated too early in the analyses. The maximum load at which the analyses terminated is seen to be much lower than the experimental failure load data.

Artificial Damping Effects on Failure Load Prediction

We performed multiple analyses using a different level of artificial damping parameter, b_0 , for each of the small coupon problems. Figure 7-6 plots some of these results, which shows the effects of the artificial damping parameter on the final failure load prediction.

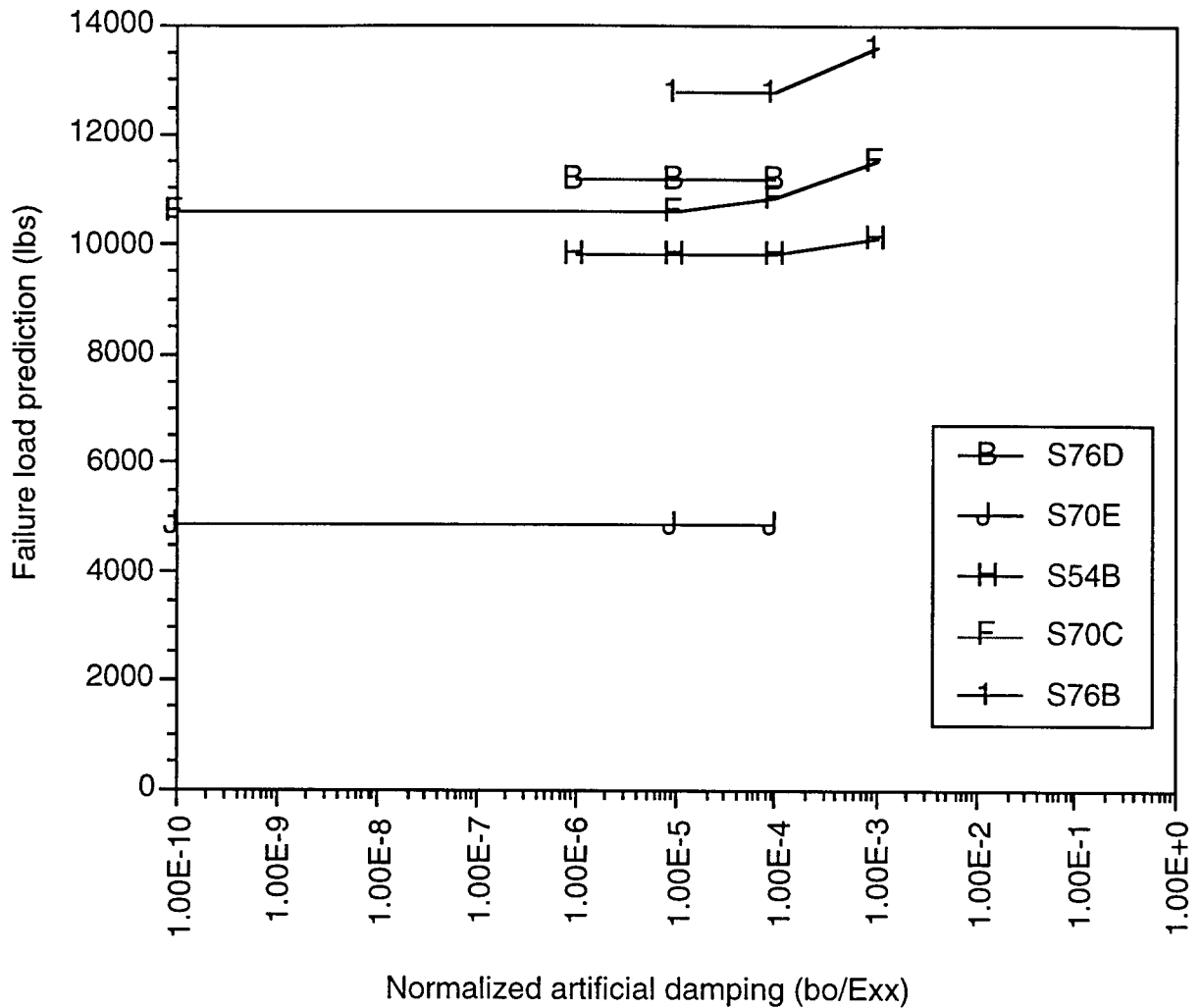


Figure 7-6. Damping effects on small coupon failure prediction.

These results show that for small coupons, some analyses did not have any nonconvergence problems, and some analyses only needed a very small level of artificial damping to overcome nonconvergence problems. Furthermore, for analyses that did use artificial damping to overcome nonconvergence problems, the artificial damping did not have any significant effects on the failure load predictions.

7.2 Large Panel Verification

Data from several large panel experiments were used to verify failure load prediction of the damage with artificial damping model. There were five uniaxial tension data and two biaxial tension data. These test data were obtained from the Boeing Company [5,51].

Experimental Data

Figure 7-7 shows a schematic of the large panel under uniaxial tension test case. Table 7-4 shows the dimensions, material, and lay-ups of the five test cases. The width of the slit for all five cases was 0.070 inch.

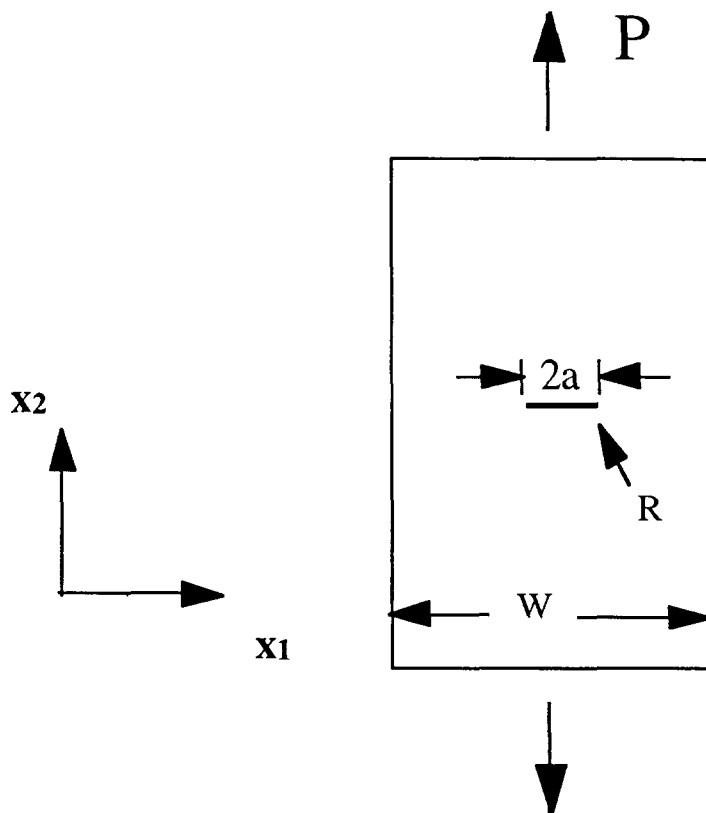


Figure 7-7. Schematic of large panel under uniaxial tension load.

Table 7-4. Large panels under uniaxial tension test cases.

| Case | W (in.) | 2a (in.) | Material | Lay-up |
|------|------------|-------------|------------|---|
| P8 | 36 | 8 | IM7/8551-7 | $[\pm 45/90/0/\pm 60/\bar{90}]_s$ |
| P9A | 36 | 9 | IM7/8551-7 | $[\pm 45/0/90/\pm 30/\bar{0}]_s$ |
| P9B | 36 | 9 | AS4/938 | $[\pm 45/0/90/\pm 30/\bar{0}]_s$ |
| P12A | 60 | 12 | AS4/938 | $[\pm 45/0/90/\pm 30/\bar{0}]_s$ |
| P12B | 60 | 12 | AS4/938 | $[\pm 45/90/0/\pm 60/15/90/-15/\mp 60/0/90/\mp 45]_s$ |

Figure 7-8 shows the basic configuration of the biaxial tension test. There were two sets of test data. Table 7-5 summarizes these two tests.

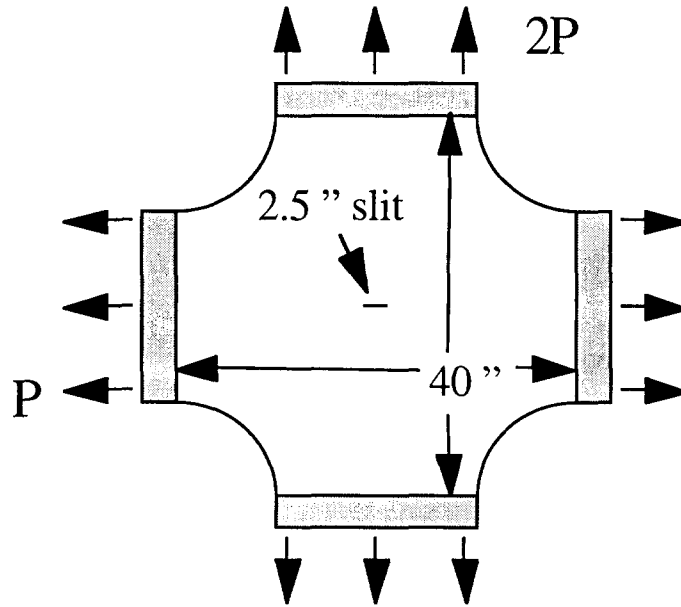


Figure 7-8. Large panel under biaxial tension tests.

Table 7-5. Biaxial panel test cases.

| Case | Material | Lay-up |
|------|------------------|-------------------------|
| iax1 | B A S4/938 | $[45/0/-45/0/90/0]_s$ |
| iax2 | B A S4/938 | $[-45/90/45/90/0/90]_s$ |

Progressive Damage Analyses

Finite element analyses using both the damage with damping model and the damage model alone were performed for the large panels. These analyses were of the same type with those of the small coupon cases. In simplifying the analyses, symmetry conditions about the x_2-x_3 plane were assumed, and only half of the geometry were modeled. The external load for the uniaxial panel analyses was displacement controlled.

The load for the biaxial analyses was load controlled. Table 7-6 shows the properties used in the analyses for the large panel cases. Figure 7-9 shows the mesh used for the biaxial analyses

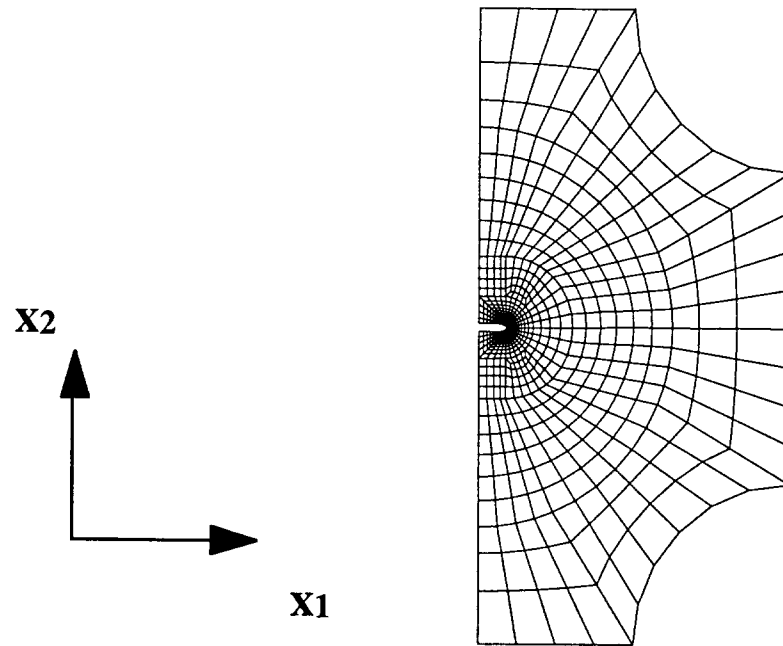


Figure 7-9. Biaxial mesh.

Table 7-6. Properties and parameters used in large panel analyses.

| Properties | IM7/8551-7 | AS4/938 |
|--------------------|---------------|----------|
| <u>Moduli</u> | | |
| E_x (msi) | 20.2 | 21.0 |
| E_y (msi) | 1.43 | 1.39 |
| ν_{xy} | 0.30 | 0.31 |
| G_{xy} (msi) | 0.76 | 0.69 |
| $\alpha(1/psi^3)$ | 8.0e-15 [48] | 1.0e-14 |
| G_{yz} (msi) | 0.61 [52] | 0.61 |
| G_{xz} (msi) | 0.76 | 0.69 |
| <u>Other</u> | | |
| <u>Properties</u> | | |
| $\alpha_x(1/F)$ | -0.17e-6 [52] | -0.17e-6 |
| $\alpha_y(1/F)$ | 15.6e-6 [52] | 15.6e-6 |
| $T_{cure}(F)$ | 267 [52] | 340 |
| $T_{room}(F)$ | 75 | 75 |
| X_t (ksi) | 320 | 222 [53] |
| δ (in.) | 0.0052 | 0.005 |
| G_{Ic} (lb/in.) | 1.00 | 0.85 |
| G_{IIc} (lb/in.) | 2.00 | 1.70 |
| h (in.) | 0.0074 | 0.007 |
| τ_v | 0.03 | 0.03 |
| τ_r | 0.05 | 0.05 |

Failure Load Comparison

Table 7-7 shows the failure load comparisons between experimental data and predictions using both the damage with damping model and the damage model alone. Predictions for the damage model alone were based on maximum load in the analyses since these analyses terminated before final failures due to nonconvergence problems. Figure 7-10 plots the two predictions normalized with experimental data. Again, predictions using the damage model alone represented existing modeling methods. Predictions using both the damage model and the damping model represented new capability from this study.

Table 7-7. Failure load comparison for large panels.

| Case | Test Data (lb) | Damage/ Damage (lb) | Damage (lb) |
|-------------|---------------------------|--------------------------------|------------------------|
| P8 | 78,000 | 80,000 | 43,000 |
| P9A | 71,000 | 77,000 | 38,000 |
| P9B | 64,000 | 70,000 | 59,500 |
| P12A | 135,000 | 118,000 | 70,000 |
| P12B | 150,000 | 135,000 | 56,000 |
| Biax1 | 100,000 | 115,000 | 54,000 |
| Biax2 | 100,000 | 95,000 | 48,000 |

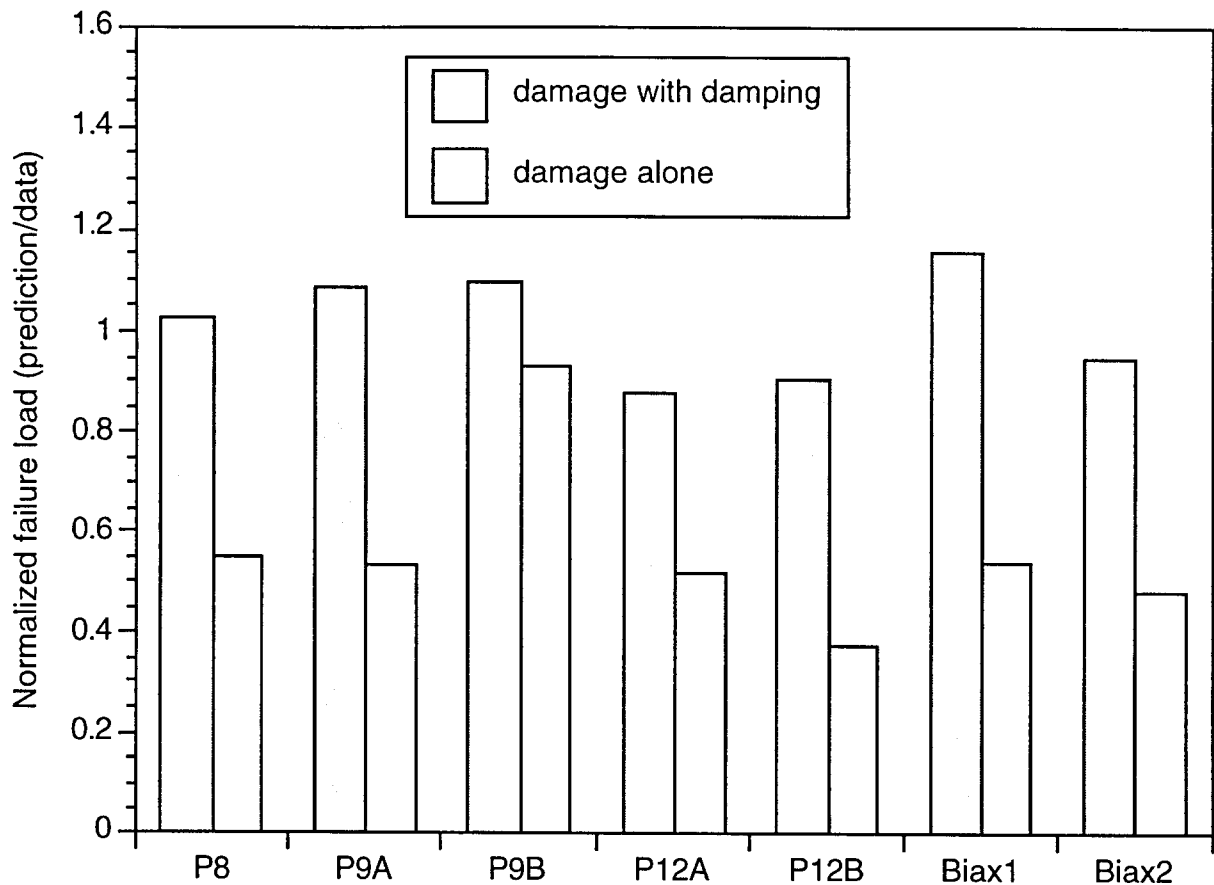


Figure 7-10. Fracture strength comparison for large panels.

These results show that the damage with damping model predicted failure load of large panels with more complex geometry reasonably well. Without the artificial damping, the damage model alone could not overcome nonconvergence problems and stopped too early in the analyses. The maximum loads at which the analyses terminated are seen to be much lower than the experimental failure load data.

Artificial Damping Effects on Failure Load Prediction

Figure 7-11 shows the effects of damping on failure load prediction for some of the large panel analyses. It is seen that very large changes in the artificial damping parameter only had little effects on the failure load predictions.

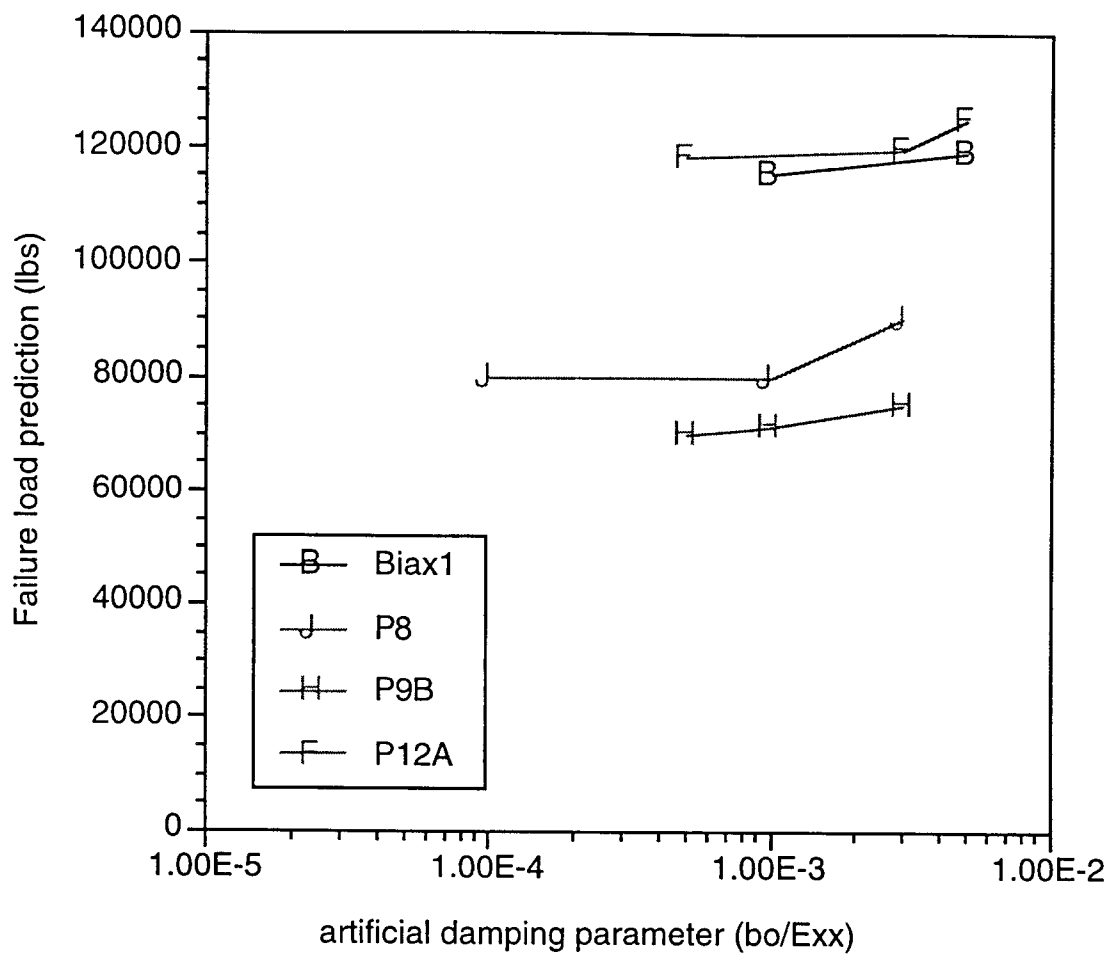


Figure 7-11. Damping effects on large panel failure predictions.

Chapter 8

Summary and Discussions

An analytical method that can effectively predict the fracture strength of composite plates containing damages is a much needed modeling capability. This type of modeling is required for damage tolerance analyses of composite pressure vessels. Existing modeling methods, including failure criteria based on fracture mechanics and finite element analyses using progressive damage models (progressive damage analyses), are not effective. The fracture criteria are expensive and lack accuracy. The progressive damage analyses have serious numerical difficulty in modeling brittle failures of composites. The current research objective was to develop a damage model that can be used with current finite element codes to predict the failure load of damaged composite shells subjected to in-plane tension load.

There are two difficulties involved with using progressive damage analyses. First, the composite progressive damage model must capture the relevant damage mechanics. Second, the finite element analyses must model brittle composite failures as defined by the progressive damage models. The focus of this research is on overcoming the numerical difficulty caused by brittle composite failures.

Problems involving predicting failure composite plates with damages are very difficult to model. These difficulties arise because of the physics of these problems include both slow rate regime (quasi-static to structural dynamic), and very high rate (wave propagation) regime. This study considered only quasi-static loading problems, such as the slow pressurization of a pressure vessel. For such a case, most of the problem is in the slow loading regime, but when brittle failures occurred, they created shocks in the structures. These shocks are in high rate regime. Slow rate regime problems work best with implicit integration schemes. However, current finite element codes cannot handle both of these regimes in the same analysis. This problem renders the progressive damage analyses ineffective against failure modeling of composite structures.

Analyses that use a slow rate solution scheme, an implicit integration scheme, will usually encounter serious numerical difficulties when shocks occur and will terminate prematurely. These difficulties are failures of the solution scheme in finding a displacement field that will satisfy equilibrium requirements within some given tolerances. Basically, the time step taken by the slow rate scheme is too large when the problem is in the shock regime. On the other hand, analyses that use a high rate solution scheme, an explicit integration scheme, will cost too much because these schemes require relatively small time step, and the majority of these plate problems is in the slow rate regime.

Instead of solving these real problems, the current research changed these problems into easier problems that can be solved with current finite element capabilities. To obtain the easier problems, the current research uses a slow rate solution scheme and adds artificial damping to the material model. The artificial damping suppresses the shocks caused by brittle fiber failures and keeps the finite element analyses in the slow rate regime. This allows the analyses to overcome nonconvergence problems so that the analyses can be finished and the final failure load can be predicted. In doing this, the modeling method relies on a very important assumption. The assumption is that the added artificial damping will overcome the nonconvergence problems without significantly changing the final failure load prediction, the desired analysis results.

The validity of this modeling with artificial method depends on the accuracy of the above assumption. The accuracy of this assumption varies from problem to problem. There is not a prior knowledge of this assumption accuracy. However, this accuracy may be determined by using multiple analyses for the same problem at different levels of artificial damping (a parametric study).

In ideal problems, the parametric study will show that the above assumption is accurate. Thus, the artificial damping had little effects on the final failure load predictions. In troublesome problems, the parametric study will show that the above assumption is inaccurate, and the predictions can not be used. The model in the current study was developed to maximize the chance for this key assumption to be accurate.

The developed model is easy to use and can be easily implemented into standard finite element codes. The model also simplifies required parametric studies by limiting the damping model to only one active parameter, the damping level. Furthermore, values for the damping level to be used are automatically estimated from the analyses. Thus, no experiment or calculation is required to determine the damping level prior to the analyses.

The active model parameter, the damping level, is not a parameter to “calibrate” the failure prediction of the model. In fact, the key assumption, which is required for the artificial damping model, is accurate only when this damping level has little or no effect on the failure load prediction.

The cost of this modeling with artificial damping method depends on the number of analyses required to determine the effects of the artificial damping on the final failure load prediction. In ideal problems, this number could be as low as two. On the other hand, if the artificial damping has too much effect on the final failure load,

then the final failure predictions cannot be used. In these cases, all analyses performed for such problems are wasted.

The current study tested the effectiveness of the modeling with damping method using two sets of fracture strength experimental data. The first set involves small coupons with small cutouts. The second set involves large panels with larger cutouts.

For the small coupons, there was little fiber failure propagation before the final failure occurred. Both progressive damage models, with the artificial damping and without the artificial damping, predicted the coupons' fracture strength well. However, all analyses with the artificial damping finished properly, where some of the analyses without the artificial damping stopped before the final failure load was predicted due to nonconvergence problems. In small coupon analyses with nonconvergence problems, the fracture strength was simply calculated from the maximum load in the analyses. This practice seemed to work for small coupons since there was very little failure propagation before the final failure; the final failure load was very close to the maximum load in analyses with nonconvergence problems. For these small coupons, parametric studies showed that the assumption that the artificial damping does not have significant effects on the failure load.

For the large panels, analyses without artificial damping terminated prematurely due to nonconvergence problems at about half of the experimental failure load data. Analyses with artificial damping predicted the final failure load reasonably close to the experimental failure load data. From the analyses' results, it was seen that there was much more fiber failure progressions in the analyses with artificial damping than in analyses without artificial damping. For these large panels, parametric studies showed that the assumption that the artificial damping does not have significant effects on the failure load, and predictions were reasonably accurate.

For the two verification data sets used in this study, the modeling with artificial damping was effective in predicting the fracture strength of composite plates subjected to in-plane tension loads. These results showed promising potential for this modeling method. More verifications, especially for more complex geometry and loading, are needed to further assess the usefulness of this modeling method.

The artificial damping model was developed and verified for the selected damage model. However, this damping modeling method can be applied to other composite damage models. When applied to other damage model, the artificial damping model should be tailored to the degradation characteristics of the damage model under consideration.

Before this study, analytical methods for predicting the fracture strength of composite plates subjected to in-plane loading were simply ineffective. For practical problems, progressive damage analyses will encounter severe numerical problems due to the brittle nature of composite failures. These numerical problems prevent the analyses from obtaining reasonable fracture strength predictions. This study developed a modeling method that can help progressive damage analyses to overcome these numerical problems. Thus, the developed modeling method has advanced the modeling technology for these composite fracture problems.

Appendix A

Extensional Viscous Stiffness Matrix

§A.1 Constitutive Equations for Unidirectional Composites

This appendix summarizes equations for calculating the extensional viscous stiffness matrix A' . These equations are the same as those for calculating the familiar extensional stiffness matrix A [24,26].

This study only considers composite laminates comprised of unidirectional plies. Figure A-1 shows coordinate systems for unidirectional composites.

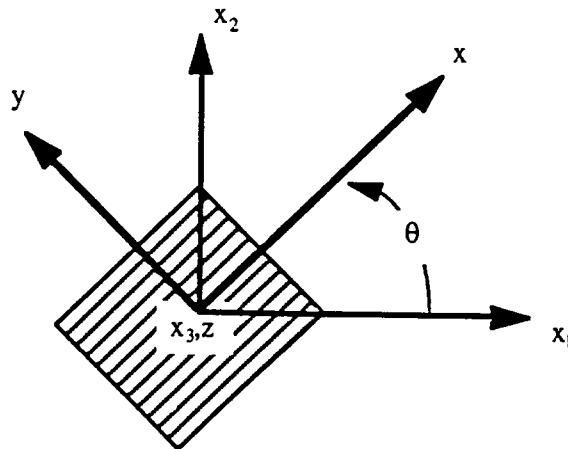


Figure A-1 On-axis (x, y, z) and off-axis (x_1, x_2, x_3) coordinate systems.

Based on the plane stress assumption, only three in-plane components of stress and strain are used in this study. Defining the on-axis plane stress and strain matrix as:

$$\boldsymbol{\sigma}^{local} = \begin{Bmatrix} \sigma_{xx} \\ \sigma_{yy} \\ \sigma_{xy} \end{Bmatrix} \quad (A.1)$$

$$\boldsymbol{\epsilon}^{local} = \begin{Bmatrix} \epsilon_{xx} \\ \epsilon_{yy} \\ \gamma_{xy} \end{Bmatrix} \quad (A.2)$$

where the superscript *local* indicates the on-axis coordinate system (local x-y). γ_{xy} is the engineering shear strain. The on axis stress-strain relations of a unidirectional ply are as follows:

$$\begin{Bmatrix} \sigma_{xx} \\ \sigma_{yy} \\ \sigma_{xy} \end{Bmatrix} = \begin{pmatrix} Q_{xx} & Q_{xy} & 0 \\ Q_{yx} & Q_{yy} & 0 \\ 0 & 0 & Q_{ss} \end{pmatrix} \begin{Bmatrix} \epsilon_{xx} \\ \epsilon_{yy} \\ \gamma_{xy} \end{Bmatrix} \quad (A.3)$$

Using matrix notation, Equation A.3 is written as:

$$\boldsymbol{\sigma}^{local} = \mathbf{Q}^{local} \boldsymbol{\epsilon}^{local} \quad (A.4)$$

where \mathbf{Q}^{local} is the on-axis stiffness matrix. The components of \mathbf{Q}^{local} are calculated as follows:

$$Q_{xx} = E_{xx}/(1 - \nu_{xy}\nu_{yx})$$

$$Q_{yy} = E_{yy}/(1 - \nu_{xy}\nu_{yx})$$

$$Q_{xy} = \nu_{yx}E_{xx}/(1 - \nu_{xy}\nu_{yx}) \quad (A.5)$$

$$Q_{yx} = \nu_{xy}E_{yy}/(1 - \nu_{xy}\nu_{yx})$$

$$Q_{ss} = G_{xy}$$

where E_x and E_y are Young's moduli in the x and y directions, respectively. ν_{xy} and ν_{yx} are Poisson's ratios. ν_{xy} measures the transverse strain in the y direction when the material is stressed only in the x direction. ν_{yx} measures the strain in the x direction when the material is stressed only in the y direction.

The global stress, strain and stiffness are:

$$\boldsymbol{\sigma}^{global} = \begin{Bmatrix} \sigma_{11} \\ \sigma_{22} \\ \sigma_{12} \end{Bmatrix} \quad (A.6)$$

$$\boldsymbol{\epsilon}^{global} = \begin{Bmatrix} \epsilon_{11} \\ \epsilon_{22} \\ \gamma_{12} \end{Bmatrix} \quad (A.7)$$

$$\mathbf{Q}^{global} = \begin{pmatrix} Q_{11} & Q_{12} & Q_{16} \\ Q_{21} & Q_{22} & Q_{26} \\ Q_{61} & Q_{62} & Q_{66} \end{pmatrix} \quad (A.8)$$

where the superscript *global* in σ^{global} , ϵ^{global} and Q^{global} denotes the global off-axis stress, strain and stiffness respectively. The global stress-strain relations are:

$$\sigma^{global} = Q^{global} \epsilon^{global} \quad (A.9)$$

On axis stress can be transformed to off-axis stress as follows [24,26]:

$$\sigma = \mathbf{T}^{-1} \sigma^l \quad (A.10)$$

where the transformation matrix \mathbf{T} is calculated as:

$$\mathbf{T} = \begin{pmatrix} \cos^2\theta & \sin^2\theta & 2\sin\theta\cos\theta \\ \sin^2\theta & \cos^2\theta & -2\sin\theta\cos\theta \\ -\sin\theta\cos\theta & \sin\theta\cos\theta & \cos^2\theta - \sin^2\theta \end{pmatrix} \quad (A.11)$$

in which θ is the orientation of the ply under consideration (see Fig. A-1). The strain ϵ^{global} and ϵ^{local} contain engineering shear strain and not tensorial shear strain. The transformation from global to local coordinates for the strain is:

$$\epsilon^{local} = \mathbf{T}^{-T} \epsilon^{global} \quad (A.12)$$

Combining Equation A.4, A.10, and A.12, the on-axis to off-axis stiffness matrix relation is calculated as:

$$Q^{global} = \mathbf{T}^{-1} Q^{local} \mathbf{T}^{-T} \quad (A.13)$$

The components of \mathbf{Q}^{global} are:

$$\begin{aligned}
Q_{11} &= Q_{xx}\cos^4\theta + 2(Q_{xy} + 2Q_{ss})\sin^2\theta\cos^2\theta + Q_{yy}\sin^4\theta \\
Q_{12} &= (Q_{xx} + Q_{yy} - 4Q_{ss})\sin^2\theta\cos^2\theta + Q_{xy}(\sin^4\theta + \cos^4\theta) \\
Q_{22} &= Q_{xx}\sin^4\theta + 2(Q_{xy} + 2Q_{ss})\sin^2\theta\cos^2\theta + Q_{yy}\cos^4\theta \\
Q_{16} &= (Q_{xx} - Q_{xy} - 2Q_{ss})\sin\theta\cos^3\theta + (Q_{xy} - Q_{yy} + 2Q_{ss})\sin^3\theta\cos\theta \\
Q_{26} &= (Q_{xx} - Q_{xy} - 2Q_{ss})\sin^3\theta\cos\theta + (Q_{xy} - Q_{yy} + 2Q_{ss})\sin\theta\cos^3\theta \\
Q_{66} &= (Q_{xx} + Q_{yy} - 2Q_{xy} - 2Q_{ss})\sin^2\theta\cos^2\theta + Q_{ss}(\sin^4\theta + \cos^4\theta)
\end{aligned} \tag{A.14}$$

§A.2 Extensional Elastic Stiffness Matrix

For flat plates subjected to in-plane tension load, the in-plane strain-displacement relations are:

$$\begin{Bmatrix} e_1^o \\ e_2^o \\ e_6^o \end{Bmatrix} = \begin{Bmatrix} \epsilon_{11} \\ \epsilon_{22} \\ \epsilon_{12} \end{Bmatrix}_{in-plane} = \begin{Bmatrix} \frac{\partial u_1}{\partial x_1} \\ \frac{\partial u_2}{\partial x_2} \\ \frac{\partial u_1}{\partial x_2} + \frac{\partial u_2}{\partial x_1} \end{Bmatrix} \tag{A.15}$$

where u_1 and u_2 are displacement in the x_1 and x_2 direction respectively. e_i^o are the membrane strain of the plate. Figure A-2 shows the laminate z (thickness) coordinate convention.

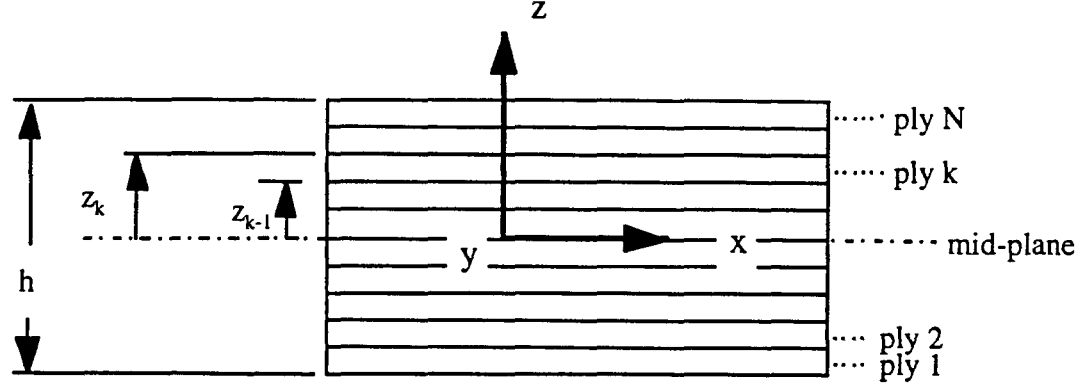


Figure A-2 Laminate's z coordinate (thickness direction).

The global stress-strain relations in the k^{th} layer of a laminate under in-plane load has the form:

$$\begin{Bmatrix} \sigma_1^k \\ \sigma_2^k \\ \sigma_6^k \end{Bmatrix} = \begin{Bmatrix} \sigma_{11}^k \\ \sigma_{22}^k \\ \sigma_{12}^k \end{Bmatrix} = \begin{pmatrix} Q_{11}^k & Q_{12}^k & Q_{16}^k \\ Q_{21}^k & Q_{22}^k & Q_{26}^k \\ Q_{61}^k & Q_{62}^k & Q_{66}^k \end{pmatrix} \begin{Bmatrix} e_1^o \\ e_2^o \\ e_6^o \end{Bmatrix} \quad (A.16)$$

The resultant forces in the plate are obtained by integrating the stresses in each layer through the thickness of the laminate:

$$\begin{Bmatrix} N_1 \\ N_2 \\ N_6 \end{Bmatrix} = \int_{-h/2}^{h/2} \begin{Bmatrix} \sigma_1 \\ \sigma_2 \\ \sigma_6 \end{Bmatrix} dz = \sum_{k=1}^N \int_{z_{k-1}}^{z_k} \begin{Bmatrix} \sigma_1^k \\ \sigma_2^k \\ \sigma_6^k \end{Bmatrix} dz \quad (A.17)$$

From Equations A.16 and A.17, the stress resultants and in-plane strain relations are:

$$\begin{Bmatrix} N_1 \\ N_2 \\ N_6 \end{Bmatrix} = \sum_{k=1}^N \int_{z_{k-1}}^{z_k} \begin{pmatrix} Q_{11}^k & Q_{12}^k & Q_{16}^k \\ Q_{21}^k & Q_{22}^k & Q_{26}^k \\ Q_{61}^k & Q_{62}^k & Q_{66}^k \end{pmatrix} \begin{Bmatrix} e_1^o \\ e_2^o \\ e_6^o \end{Bmatrix} dz \quad (A.18)$$

Since Q_{ij}^k are constant in ply k and can be moved outside of the integration. Also, the in-plane strain is constant through out the thickness. Thus, Equation A.18 can be rewritten as:

$$\begin{Bmatrix} N_1 \\ N_2 \\ N_6 \end{Bmatrix} = \begin{pmatrix} A_{11} & A_{12} & A_{16} \\ A_{21} & A_{22} & A_{26} \\ A_{16} & A_{26} & A_{66} \end{pmatrix} \begin{Bmatrix} e_1^o \\ e_2^o \\ e_6^o \end{Bmatrix} \quad (\text{A.19})$$

in which:

$$A_{ij} = \sum_{k=1}^N Q_{ij}(z_k - z_{k-1}) \quad (\text{A.20})$$

§A.3 Extensional Viscous Stiffness

For the artificial damping model, the calculations of the extensional viscous stiffness, denotes as \mathbf{A}' , are the same way as the calculations of extensional elastic stiffness. From the model developed in Chapter 6, the on axis stress-strain rate relations are:

$$\begin{Bmatrix} \sigma_{xx} \\ \sigma_{yy} \\ \sigma_{xy} \end{Bmatrix}_{damping} = \begin{pmatrix} b(s_f, \tau) & 0 & 0 \\ 0 & 0 & 0 \\ 0 & 0 & 0 \end{pmatrix} \begin{Bmatrix} \dot{\epsilon}_{xx} \\ \dot{\epsilon}_{yy} \\ \dot{\gamma}_{xy} \end{Bmatrix} \quad (\text{A.21})$$

where the fiber failure state variable s_f , the analysis “time” τ and the strain rate are defined in Chapter 6. Equation A.21 can be rewritten in matrix form as:

$$\sigma_{damping}^{local} = \mathbf{Q}_{damping}^{local} \dot{\epsilon}^{local} \quad (\text{A.22})$$

In global coordinates:

$$\sigma_{damping}^{global} = \mathbf{Q}_{damping}^{global} \dot{\epsilon}^{global} \quad (A.23)$$

The stress, strain, and stiffness transformations are the same for the viscous components as for the elastic components. Thus the viscous stiffness transformation is:

$$\mathbf{Q}_{damping}^{global} = \mathbf{T}^{-1} \mathbf{Q}_{damping}^{local} \mathbf{T}^{-T} \quad (A.24)$$

From Equations A.14, A.21 and A.3, the components of $\mathbf{Q}_{damping}^{global}$ are:

$$\begin{aligned} Q'_{11} &= b(s_f, \tau) \cos^4 \theta \\ Q'_{12} &= b(s_f, \tau) \sin^2 \theta \cos^2 \theta \\ Q'_{22} &= b(s_f, \tau) \sin^4 \theta \\ Q'_{16} &= b(s_f, \tau) \sin \theta \cos^3 \theta \\ Q'_{26} &= b(s_f, \tau) \sin^3 \theta \cos \theta \\ Q'_{66} &= b(s_f, \tau) \sin^2 \theta \cos^2 \theta \end{aligned} \quad (A.25)$$

where the ' denotes artificial damping components. The force resultants due to damping are also calculated in the same manner as for the elastic force resultants. Furthermore, since the strain rate are independent of the thickness coordinate, the viscous form of Equation A.19 can be written as:

$$\begin{Bmatrix} N'_1 \\ N'_2 \\ N'_6 \end{Bmatrix} = \begin{pmatrix} A'_{11} & A'_{12} & A'_{16} \\ A'_{21} & A'_{22} & A'_{26} \\ A'_{16} & A'_{26} & A'_{66} \end{pmatrix} \begin{Bmatrix} \dot{e}_1^o \\ \dot{e}_2^o \\ \dot{e}_6^o \end{Bmatrix} \quad (A.26)$$

in which:

$$A'_{ij} = \sum_{k=1}^N Q'_{ij}(z_k - z_{k-1}) \quad (A.27)$$

This page intentionally left blank

Appendix B

Using PDLAM with ABAQUS/Standard

The composite damage material model developed in Chapter 4 and the artificial damping model developed in Chapter 6 was implemented into a material user subroutine called PDLAM. PDLAM can be used with ABAQUS/Standard to predict the tension fracture of composite plates. This appendix summarizes preparations required for using PDLAM with ABAQUS. The user is assumed to be familiar with using ABAQUS.

B.1 Overview

ABAQUS calls PDLAM to get the material behavior in an analysis. PDLAM requires various data to perform the material modeling. PDLAM receives data from ABAQUS/Standard during the analysis and from external files generated before the analysis start. There are two preparations required to use PDLAM with ABAQUS/Standard. First, the user needs to perform some preprocessing to generate the external data files for PDLAM. Second, the user needs to prepare the ABAQUS input file to work with PDLAM.

B.2 Preprocessing for PDLAM

PDLAM requires data input from external files that are generated before the start of the finite element analysis. These external files are obtained by running preprocessing programs. Table B-1 summarizes the required external files, their contents, and the programs that can generate these files.

Table B-1. External files required for PDLAM.

| File | Contents | Program |
|--------------------------------|---|---------|
| ply <i>i</i> .OUT ^a | $Q(\varphi)$, $Y(\varphi)$, $S(\varphi)$ for ply <i>i</i> | PDCOMP |
| pdens.OUT plies | saturation crack density for all plies | PDCOMP |
| rsde.OUT plies | residual thermal strain for all plies | RSDE |
| area.OUT | element surface area | VAREA |

^a*i* = 1,2,..., number of ply in laminate.

To run PDCOMP, the user must prepare an input file called pdcomp.inp. This input file requires laminate data, material properties and parameters for PDCOMP. Documentation for preparing pdcomp.inp and running PDCOMP can be obtained from [21].

The user must execute PDCOMP before executing RSDE because PDCOMP generates the file prsde.OUT that is used as input for RSDE. VAREA is a user friendly program that calculates element area for flat plates from nodal coordinates and element connectivity data in the ABAQUS input file.

B.3 ABAQUS Input File Preparation for PDLAM

PDLAM was developed to be used with layered shells (S4R, S4R5, S8R, S8R5, etc. in ABAQUS). For layered shells, the *SHELL SECTION, *ORIENTATION, and *MATERIAL commands are used to define the lay-up, layer thicknesses, layer local orientation, and layer material.

The *USER MATERIAL command tells ABAQUS to use a user defined material subroutine. The lines following this command are used to provide data to the material subroutine during the ABAQUS analysis. PDLAM reserves 32 space for data input from ABAQUS. Table B-2 lists the required data for PDLAM.

The *DEPVAR command tells ABAQUS to reserve space for solution dependent state variables for the material point. PDLAM reserves 20 state variable spaces. Not all 20 spaces are used.

Table B-2. Data for PDLAM through ABAQUS input file.

| Data ^a | Description |
|-------------------|---|
| 1 | E_{xx} |
| 2 | E_{yy} |
| 3 | ν_{xy} |
| 4 | G_{xy} |
| 5 | X_T , longitudinal tensile strength |
| 8 | α , shear nonlinearity parameter |
| 9 | number of ply |
| 11 | number of element |
| 18 | $\Delta\phi$ \Delta \phi, crack density increment |
| 19 | δ \delta, fiber interaction length |
| 30 | τ_v \tau_{v}, full damping period |
| 31 | b_0 , initial artificial damping level |
| 32 | τ_r , damping ramp down period |

^aUnlisted numbers are inactive data.

This page intentionally left blank

References

- [1] Military Standard 1530A (USAF), *Air structural integrity program, airplane requirements*, August 1, 1975.
- [2] Anderson, T.L., *Fracture Mechanics: Fundamentals and Applications*, Second Edition, CRC Press Inc., Ann Arbor, 1995.
- [3] Ilcewicz, L.B., Walker, T.H., Murphy, D.B., Dopker B., Scholz, D.B., Cairns, D.S., Poe, C.C.Jr, "Tension Fracture of Laminates for Transport Fuselage, Part IV: Damage Tolerance Analysis," Fourth NASA/DoD Advanced Technology Conference, NASA CP 3229,1993, pp. 243-264.
- [4] Walker, T.H., et. al., "Tension Fracture of Laminates for Transport Fuselage, Part I: Material Screening," Second NASA Advanced Technology Conference, NASA CP 3154,1991, pp. 197-238.
- [5] Walker, T.H., et. al., "Tension Fracture of Laminates for Transport Fuselage, Part II: Large Notches," Third NASA Advanced Technology Conference, NASA CP 3178,1992, pp. 277-758.
- [6] Walker, T.H., Scholz, D., Flynn, B., Dopker B., Bodine., J. Ilcewicz, L., Rouse, M., Mc.Gowan D., Poe, C.Jr, "Damage Tolerance of Composite Fuselage Structure," Sixth NASA/DoD/ARPA Advanced Technology Conference, NASA CP, Anaheim, CA, 1995.
- [7] Awerbuch, J. and Madhukar, M.S., "Notched Strength of Composite Laminates: Predictions and Experiments-A Review," *Journal of Reinforced Plastics and Composites*, Vol. 4, 1985, pp. 1-159.
- [8] Waddoups, M.E., Eisenmann, J.R., and Kaminski, B.E., "Macroscopic Fracture Mechanics of Advanced Composite Materials," *Journal of Composite Material*, Vol. 5, 1971, pp. 446-454.
- [9] Whitney, J.M. and Nuismer, R.J., "Stress Fracture Criteria for Laminated Composites Containing Stress Concentrations," *Journal of Composite Materials*, Vol. 8, 1974, pp. 253-265.
- [10] Nuismer, R.J. and Whitney, J.M., "Uniaxial Failure of Composite Laminates Containing Stress Concentrations," *Fracture Mechanics of Composites*, ASTM STP 593,1975, pp. 117-142.
- [11] Poe, C.C., Jr. and Sova, J.A., "Fracture Toughness of Boron/ Aluminum Laminates with Various Porportions of 0 degree and 45 degree Plies," NASA Technical Paper 1707, 1980.
- [12] Poe, C.C., Jr. , "A Unified Strain Criterion for Fracture of Fibrous Composite Laminates," *Engineering Fracture Mechanics*, Vol. 17, No. 2, pp. 153-171, 1983.

- [13] Mar, J.W. and Lin, K.Y., "Fracture Mechanics Correlation for Tensile Failure of Filamentary Composites with Holes," *Journal of Aircraft*, Vol. 14, 1977, pp. 703-704.
- [14] Tan, S.C., "Notched Strength Prediction and Design of Laminated Composites Under In-Plane Loadings," *Journal of Composite Materials*, Vol. 21 1987, pp. 750-780.
- [15] Lagace, P.A., Bhat, N.V., and Gundogdu, A., "Response of Notched Graphite/Epoxy and Graphite/PEEK systems," *Composite Materials: Fatigue and Fracture, Fourth Volume, ASTM STP 1156*, American Society for Testing and Materials, Philadelphia, 1993, pp. 55-71.
- [16] Walker, Ilcewicz, L.B., Polland, D.R., Bodine, J.B., Poe, C.C.Jr., "Tension Fracture of Laminates for Transport Fuselage, Part III: Structural Configurations," *Fourth NASA/DoD Advanced Technology Conference, NASA CP 3229*, 1993, pp. 243-264.
- [17] Dopker, B., Murphy, D.P., Ilcewicz, L., Walker, T., "Damage Tolerance Analysis of Composite Transport Fuselage Structure," *AIAA-94-1406-CP*, 1994, pp. 803-810.
- [18] Chang, K.Y., Liu, S., and Chang, F. K. , "Damage Tolerance of Laminated Composites Containing an Open Hole and Subjected to Tensile Loading," *Journal of Composite Materials*, Vol. 25, 1991, pp. 834-855.
- [19] Shahid, I. and Chang, F. K., "An Accumulative Damage Model for Tensile and Shear Failures of Laminated Composite Plates," *Journal of Composite Materials*, Vol. 29, pp. 926-981, 1995.
- [20] Lo, D.C., Allen, D.H., Harris, C.E., "Modeling the Progressive Failure of Laminated Composites with Continuum Damage Mechanics," *Fracture Mechanics: Twenty Third Symposium, ASTM STP 1189*, Ravinder Chona, American Society for Testing and Materials, Philadelphia, 1993, pp. 680-695.
- [21] Shahid, I., "Failure and Response of Laminated Composites Subjected to In-Plane Loads," Ph.D. dissertation, Stanford University, 1993.
- [22] Chang, F. K. and Chang, K.Y. , "A Progressive Damage Model for Laminated Composite Containing Stress Concentrations," *Journal of Composite Materials*, Vol. 21, pp. 834-855, 1987.
- [23] ABAQUS is a commercial, general-purpose finite element code, Hibbit, Karlsson & Sorensen Inc., Pawtucket, Rhode Island, USA, 1997.
- [24] Tsai, S. W. and Hahn, H. T., *Introduction to Composite Materials*, Technomic Publishing Company, Inc., Pennsylvania, 1980.
- [25] Ugural, A.C., *Stresses in Plates and Shells*, McGraw-Hill Book Company, New York, 1981.

- [26] Chang, F. K., "Design of Composite Structures," AA257 Course Notes, Stanford University custom course material, Stanford Bookstore, Stanford, California, USA, 1996.
- [27] Tsai, S. W., *Composite Design*, Think Composites, Dayton, Ohio, 1988.
- [28] Hahn, H. T. and Tsai, S. W., "Shear Nonlinearity in Composites," *Journal of Composite Materials*, Vol. 8, 1973, pp. 68-85.
- [29] Rosen, B.W., "Tension Failure of Fibrous Composites," *AAIA Journal*, Vol. 2, No. 11, 1964, pp. 1985-1991.
- [30] Zweben, C., "Tension Failure of Fibrous Composites," *AAIA Journal*, Vol. 6, No. 12, 1968, pp. 2325-2331.
- [31] Zweben, C. and Rosen, B.W. , "A Statistical Theory of Material Strength with Applications to Composite Materials," *Journal of Mech. Phys. Solids*, Vol. 18, 1970, pp. 189-206.
- [32] Nahas, M. N., "Survey of Failure and Post-Failure Theories of Laminated Fiber Reinforced Composites," *Journal of Composites Technology Research*, Vol. 8, No. 4, Winter, 1986, pp. 138-153.
- [33] Hashin, Z., "Failure Criteria for Unidirectional Fiber Composites," *Journal of Applied Mechanics*, Vol. 47, 1980, pp. 329-334.
- [34] Hibbit, Karlsson & Sorensen Inc., *ABAQUS/Standard User's Manual, Volume I*, Hibbit, Karlsson & Sorensen Inc. course note, Pawtucket, Rhode Island, USA, 1995.
- [35] Hibbit, Karlsson & Sorensen Inc., *ABAQUS/Standard Theory Manual*, Hibbit, Karlsson & Sorensen Inc., Pawtucket, Rhode Island, USA, 1995.
- [36] Hibbit, Karlsson & Sorensen Inc., *ABAQUS/Standard User's Manual, Volume II*, Hibbit, Karlsson & Sorensen Inc., Pawtucket, Rhode Island, USA, 1995.
- [37] Hibbit, Karlsson & Sorensen Inc., "Writing UMATs and VumatS", Hibbit, Karlsson & Sorensen Inc., ABAQUS Users' Conference, Newport, Rhode Island, USA, 1996.
- [38] Hughes, T.J.R., *The Finite Element Method: Linear, Static and Dynamic Analyses*, Prentice-Hall Inc., New Jersey, 1987.
- [39] Fung, Y. C., *Foundations of Solid Mechanics*, Prentice-Hall Inc., New Jersey, 1965.
- [40] Hibbit, Karlsson & Sorensen Inc., *An Introduction to ABAQUS/Explicit*, Hibbit, Karlsson & Sorensen Inc. course note, Pawtucket, Rhode Island, USA, 1995.

- [41] Hughes, T.J.R., "Nonlinear Finite Element Analyses," ME235C Course Notes, Stanford University custom course material, Stanford Bookstore, Stanford, California, USA, 1996.
- [42] Cook, R. D., Malkus, D. S., Plesha, M. E., *Concepts and Applications of Finite Element Analysis*, Third Edition, John Wiley Sons, Inc., New York, 1974.
- [43] Bathe, K. J., *Finite Element Procedures*, Prentice-Hall Inc., New Jersey, 1996.
- [44] Zienkiewicz, O.C., Taylor, R.L., *The Finite Element Method: Volume 1, Basic Formulation and Linear Problems*, Fourth Edition, McGraw-Hill, London, 1989.
- [45] Zienkiewicz, O.C., Taylor, R.L., *The Finite Element Method: Volume 2, Solid and Fluid Mechanics and Non-linearity*, Fourth Edition, McGraw-Hill, London, 1989.
- [46] Hashin, Z., "Analysis of Orthogonally Cracked Laminates Under Tension," *Journal of Applied Mechanics*, Transactions ASME, Vol. 54. No. 4, 1987, pp. 872-879.
- [47] Nuismer, R. J., Tan, S. C., "Constitutive Relations of a Cracked Composite Lamina," *Journal of Composite Materials*, Vol. 22, 1988, pp. 306-321.
- [48] Hung, C. L., "Response of Mechanically Fastened Composite Joints Under Multiple Bypass Loads," Ph.D. dissertation, Stanford University. 1994.
- [49] Needleman, A., "Material Rate Dependence and Mesh Sensitivity in Localization Problems," *Compu. Methods Appl. Mech. Eng.*, 67, 1987, pp. 68-85.
- [50] Lu, W.Y., and Trinh, K. V. "An Experimental and Computational Study of Progressive Failure of Laminated Composites with Cut-outs," 10th International Conference on Composite Materials, Whistler, British Columbia, Canada, 1995.
- [51] Private communication with Walker, T.H., Renton, Washington, 1993
- [52] Varna, J. and Berglund, L. A., "A Model for Prediction of the Transverse Cracking Strain in Cross-Ply Laminates," *J. Reinforced Plastics and Composites*, Vol. 11, No. 11, 1992, pp. 708-728.
- [53] Jackson, K. E. and Kellas, S., "Effect of Specimen Size on the Tensile Strength of Geometrically Composite Laminates," pp. 1.-3.

DISTRIBUTION:

10 K. V. Trinh, LLNL, L-125

1 MS 9001 T. O. Hunter, 8000
Attn.: J. F. Ney (A), 5200
J. B. Wright, 2200
M. E. John, 8100
L. A. West, 8200
W. J. McLean, 8300
R. C. Wayne, 8400
P. N. Smith, 8500
P. E. Brewer, 8600
T. M. Dyer, 8700
D. L. Crawford, 8900

1 MS 9042 E. P. Chen, 8742

1 MS 9131 R. A. Condouris, 8815

3 MS 9018 Central Technical Files, 8940-2

4 MS 0899 Technical Library, 4916

2 MS 9021 Technical Communications Dept. 8815, for DOE/OSTI

1 MS 9021 Technical Communications Dept. 8815/Technical Library, 4916

This page intentionally left blank